

## Response to reviewer#1

The paper by Wu et al. titled "A novel study of the morphology and effective density of externally mixed black carbon aerosols in ambient air using a size-resolved single particle soot photometer (SP2)" presents measurements of the mass of rBC particles with known mobility diameters, sampled from the atmosphere of urban Beijing. A selected portion of the measurements (the most common masses for a given diameter) are interpreted in terms of two parameters commonly used in the soot community, the effective density and mass-mobility exponent (erroneously called the fractal dimension by the authors). The remainder of the measurements (the shape of the overall distribution) are not interpreted.

The manuscript as submitted represents an intelligent and detailed analysis of one aspect of the data set. However, it is not a complete analysis as discussed below, and the comprehensiveness of the work could be significantly improved. Moreover, the conclusions that the authors reach are in some ways predetermined by the analysis method. Therefore, the conclusions are misleading and the manuscript should be substantially revised. The data set shows significant promise, but before publication in AMT needs to be re-analyzed by asking the question, "what can we learn from these measurements?" instead of "how can we calculate common soot diagnostics from these measurements?"

As I explain below, the authors have accidentally only analyzed uncoated particles. It is not clear whether coated particles could be separated from multiply-charged particles using this method. Therefore, I have recommended rejection unless the authors can show that the problems of restructuring/coating and multiply charging can be separated. With this potential improvement, the paper might become a substantial contribution to the literature.

We greatly appreciate the reviewer for providing very constructive comments which have helped us improve the paper. We have considered the comments carefully and revised the manuscript accordingly, as detailed below in our point-to-point responses to the specific comments.

### Major comments

The authors have clearly thought carefully about their data and performed a careful analysis. The DMA was stepped instead of scanned, which avoids problems of data inversion otherwise associated with tandem DMA setups. My major comments are:

1. Limitations of the gaussian fitting

The authors have performed gaussian fitting to the number distributions of rBC-mass-per-particle measured by the SP2 after the DMA. But a huge part of this distribution is not described by the gaussian fit. From my estimation about 50% of particles are not described, at smaller masses. This needs to be addressed quantitatively and seriously in the analysis.

The first hypothesis for the non-gaussian shape is multiple charging. The authors blame this on the distribution change in Section 3.2. This is possibly important. But also important would be restructuring due to coatings. Larger rBC particles can have smaller mobility diameters ( $D_m$ ) after condensation of coatings (citations were given by the authors already). This would cause a tail to the right of the mode in Figure 2, as observed.

**Reply:** The particles selected by the DMA at a given voltage are generally quasi-monodisperse instead of having a single mobility diameter due to the transfer function of DMA. Thus, the peak diameter is used to represent the typical diameter of the particles selected by the DMA at the given voltage. In this study, we intend to obtain the typical mass of the externally mixed BC (extBC) particles selected by the DMA at a given voltage. Therefore, the masses corresponding to the peaks of the number distributions of rBC-mass-per-particle were required. In our original analysis, we investigated the frequency distribution of extBC mass at each prescribed mobility to obtain the peak extBC mass. However, the peak extBC mass directly obtained from the frequency distribution depends on the bin-size set in the frequency calculation. Thus, the Gaussian fitting was employed to identify the peak extBC mass with fewer artificial uncertainties.

In current study, only the peak locations of the frequency distribution of extBC mass are required. We don't concern about the practical shape of the distribution. In our original analysis, we also found that a considerable fraction of the extBC masses cannot be characterized by the Gaussian distribution, e.g., at the right tail of the distribution and the extremely small masses. The right tail beyond the Gaussian distribution can be partly interpreted by the effects of multi-charged BC particles as we discussed in the manuscript. An extBC particle having double or more charges has a larger mass than the singly charged extBC. Fig. R1 shows the frequency distribution of the incandescence peak height values of Aquadag (a representative of bare rBC for the SP2 incandescence calibration) detected by the SP2, which are proportional to the rBC masses. The Aquadag particles were well mixed in the pure water and generated by an aerosol nebulizer, and then delivered to the SP2 for measurement after passing through a diffuse dryer. Thus, the Aquadag particles were mostly without coating and considered extBC. In this case, the doubly charged Aquadag particles exhibit a clear

minor peak after the major one at a given mobility. The Gaussian fitting for the major peak can distinctly separate the singly charged particles from those with double or more charges. The multicharged Aquadag particles account ~50% of the total incandescence particles detected by the SP2 in the range of 140–250 nm in mobility diameter ( $d_{\text{mob}}$ ). The proportion gradually decreases to only a few percentage for particles larger than 600 nm  $d_{\text{mob}}$ .

However, in the case of measurement for ambient particles, it is more complex. First, the time-delay approach used in this study can only distinguish the thickly coated BC particles from the BC particles with thinly or without coating. A fraction of thinly and/or even moderately coated BC particles cannot be absolutely separated from the bare BC particles. Thus, a fraction of extBC particles claimed in this study might be thinly-coated BC particles. We propose the right tail of the distribution is also associated with the thinly coated BC particles. These thinly-coated BC particles have relatively more compact structures, resulting in larger masses than the bare BC particles at a given mobility.

As for the distribution concentrated at the smaller extBC masses, we originally considered it was resulted from the detection noises of the SP2 for the smaller BC particles. As claimed by the manufacture, the lower BC detection limit is ~0.3 fg per particle. Thus, data filter was performed by eliminating the particles with incandescence signal peak heights lower than 100. This criterion is determined from the calibration curve by using Aquadag particles (Fig. S3 in the revised supplemental file). However, the distributions concentrated at the smaller masses still exist even when the data filter is processed. Initially, we suspected the smaller masses belonged to the thickly coated BC particles which were not separated from the extBC particles using the time-delay method. However, we found that the smaller masses also existed for the bare BC particles (i.e., Aquadag). As shown in Fig. R1, the particles with these smaller masses accounted for only 1~9% of the total particle number (after data filter by eliminating the signal with incandescence peak value lower than 100) in the 140–200 nm  $d_{\text{mob}}$  range. This proportion gradually increased to ~37% at 700 nm mobility. Thus, these smaller masses should not be resulted only from the ‘remnant’ BC particles with thick coatings. We still attribute these smaller rBC masses to the measurement noises of the SP2.

In our revised manuscript, we make an improvement in data processing by investigating the number size distribution of the rBC core in extBC particles ( $dN/d\log D_c$ , where  $D_c$  is the mass-equivalent diameter of rBC core by assuming it is a void-free sphere with  $1.8 \text{ g cm}^{-3}$  density,  $N$  is the number concentration in a given  $D_c$  range) instead of the frequency distribution of extBC mass at each prescribed mobility (Fig. 2 and Fig. S6 in the revision). This improvement would reduce the artificial uncertainties in the

determination of extBC masses roughly obtained from the frequency distribution. The effect of detection noises at the small rBC masses also appears to be weakened by using the number size distribution. The size distributions at different mobility sizes are generally used in the studies of size-resolved BC particles. For instant, Zhang et al. (2016) measured the morphology and density of internally mixed BC (In-BC for short in the reference) with SP2 and VTDMA. They used the peak diameter of the normalized volume size distribution of the In-BC core to represent the typical diameter of In-BC core at the prescribed  $d_{\text{mob}}$  selected by the DMA.

As shown in Fig. 2 and Fig. S6 in the revision, a minor peak at the right side of the major peak can also be observed at a given mobility, especially in the range with  $d_{\text{mob}}$  smaller than 400 nm. The minor peak is related to both the multiply charged extBC and the thinly coated BC particles which were also recognized as extBC by using the time-delay discrimination. To examine the effect of delay time threshold employed to discriminate extBC on the determined typical extBC mass, normalized number size distributions of extBC distinguished with delay times  $< 2.0 \mu\text{s}$  (red),  $< 1.2 \mu\text{s}$  (green) and  $< 0.4 \mu\text{s}$  (blue) are compared (Fig. S6 in the revised supplemental file). Reducing the delay time threshold results in a significant reduction in the data volume that used to calculate the distribution (Fig. S5 in the revised supplemental file) and also a reduction in the extBC number fraction at the right tail of the size distribution (more significant when delay time threshold decreases to  $0.4 \mu\text{s}$ ). Reducing the delay time threshold seems to affect little on the peak location of the size distribution, which is considered the typical mass-equivalent diameters ( $d_{\text{me}}$ ), in turn the typical mass of extBC at a given mobility. The discrepancies in the lognormal-fitted peak  $d_{\text{me}}$  by using different delay time thresholds don't exceed 3% in the current study. Similar discussion is presented in detail in Section 3.2 of our revised manuscript. It implies the typical  $d_{\text{me}}$  of extBC obtained from the peak  $d_{\text{me}}$  of the number size distribution of the rBC core in extBC particles at each mobility is reliable in our study.

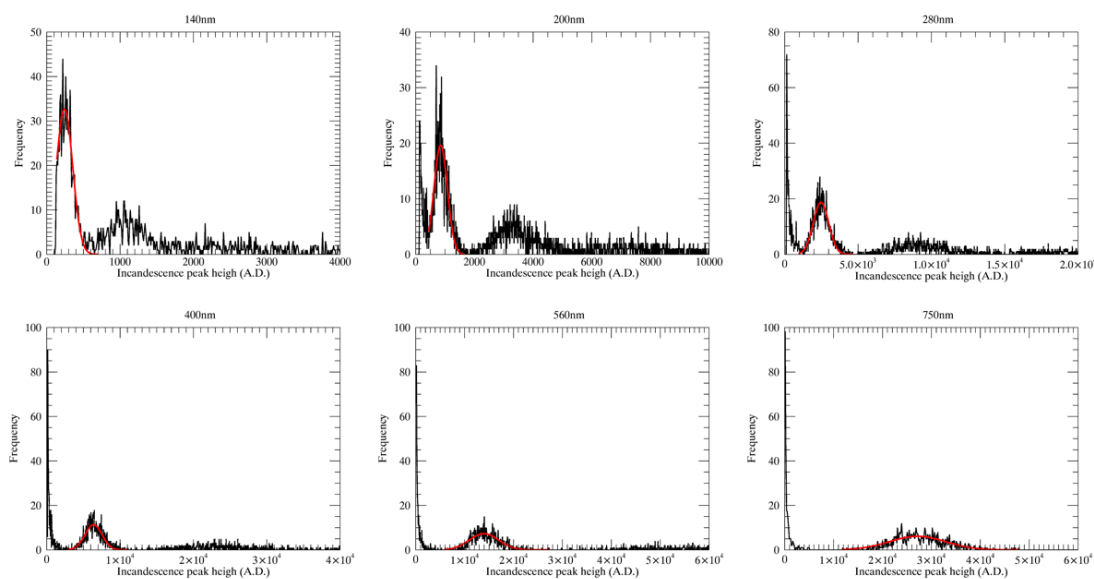


**Fig. R1** Frequency distributions of incandescence peak height detected by the SP2 for size-selected Aquadag particles at the prescribed mobility sizes. The Gaussian fitting is performed for the major peak of each distribution to obtain the typical incandescence peak height at the corresponding mobility size.

The hypothesis of coatings means that the authors' selection of the mode diameter resulted in their analysis of fresh, uncoated particles only. Therefore it is no surprise that the results indicate consistency with literature reports of fresh, uncoated particles. Therefore, the authors' results, conclusions and abstract must be rewritten.

**Reply:** The initial purpose of our experimental setup is to study the microphysical and optical properties of size-resolved BC aerosols, including the sizes, mixing states and their impacts on light absorption at different mobility sizes, as well as the morphology and effective density of extBC aggregates that presented in the current study. Similar experimental setup for the measurement of ambient BC particles can also be found in the recent literature (e.g., Zhang et al., 2016; Raatikainen et al., 2017).

Indeed, the morphology of BC aggregates has been widely studied by using different techniques, including transmission electron microscopy (TEM) and tandem measurements (e.g., DMA-APM). The morphology of diffusion-limited cluster aggregation (DLCA), to which the BC aggregates belong, has even been well documented in the review literature (Sorensen, 2011). However, as mentioned in our revised introduction, previous tandem measurements generally investigated the morphology and density of BC aggregates at small mobility sizes with the  $d_{mob}$  not exceeding 350 nm. It is likely due to the large uncertainties in the measurement for larger particles which were less abundant in the atmosphere. In our study, we use a

DMA-SP2 tandem system to study the mass-mobility relationship in a much larger mobility size range (140–750 nm) based on the sensitive and accurate SP2 measurement. The morphology and effective density determined in the relatively larger size range (140–750 nm) is compared to those in the smaller range (~50–350 nm) in the literature to examine the applicability of mass-mobility relationship established at the smaller range in previous tandem measurements. In addition, variation in the morphology and effective density of ambient extBC aggregates in the atmosphere is also studied by comparing the mass-mobility relationship in a polluted episode to that a clean period. Although the DMA-SP2 is not a novel system (Gysel et al., 2011, 2012; Zhang et al., 2016; Raatikainen et al., 2017; and other associated references cited in our revised manuscript), this tandem system is seldom used to study the microphysical properties of ambient extBC aggregates which are also abundant in the atmosphere. Especially, similar studies are deficient in urban Beijing, where the particulate pollution is severe in recent years.

We have modified our manuscript substantially. Almost all the sections are rewritten.

It would be very interesting, for example, if the fraction of restructured particles could be separated from the fraction of multiply charged particles. This is also very difficult and may be impossible. I am not certain that it is impossible, but a very convincing argument would be required to show that the two problems could be separated.

**Reply:** It is very difficult or even impossible to separate the fraction of restructured particles from the fraction of multiply charged particles. We have no idea how to deal with this issue, at least at the current stage. However, this problem should not have substantive impact on the results presented in current study. As mentioned above, the peak  $d_{me}$  (i.e., mass) of the number size distribution of the rBC core in extBC particles were required and considered the typical  $d_{me}$  (i.e., mass) of extBC at the prescribed mobility. Both the fractions of restructured particles due to thin coating and multicharged particles should only affect the shape of the distribution, e.g., cause an increase in the number size distribution at its right tail. They have few impacts on the peak location of the distribution as presented above by examining the effect of delay time threshold chosen to discriminate extBC particles.

I would like to note that the hypothesis of multiple charging would mean that smaller  $D_m$  should have a smaller fraction of total SP2 measurements explained by the Gaussian fit (since there are more pre-existing particles available to become multiply-charged in the DMA). From my inspection of Figure 2 I do not see a strong trend with  $D_m$ . This makes me suspect that coatings are involved, but is not strong enough

evidence for the authors to interpret the data as such.

**Reply:** The frequency distribution of the rBC mass in extBC particles has been replaced by the size distribution, because the frequency distribution is too rough to be presented in the scientific manuscript while the size distribution ( $dN/d\log D$ ) is more practical. As presented in the responses above, we have explained the reasons of the high frequency at smaller rBC masses and attributed it to the measurement noises of the SP2. These smaller rBC masses influence little of the normalized number size distribution. Meanwhile, the increase in the size distribution at its right tail is interpreted as the co-effects of multicharged extBC and thinly coated extBC particles which cannot be absolutely separated from the bare BC aggregates using the time-delay discrimination. During the data reanalysis, we also calculated the normalized size distributions of rBC core in thickly coated BC particles at the prescribed mobility sizes. As shown in Fig. R2, the rBC core of thickly coated BC (intBC for short) particles exhibit generally lower mass-equivalent diameters than extBC particles at each  $d_{mob}$ . Note that the size distributions with  $d_{mob} < 200$  nm are not presented due to the lower detection limit of the SP2. It can be expected because the mobility of the whole intBC particle, which is composed of a rBC core and a considerable non-refractory materials, was selected by the DMA while only the mass of rBC core was measured by the SP2. For extBC, the mass of particle is mostly attributed to the rBC core.

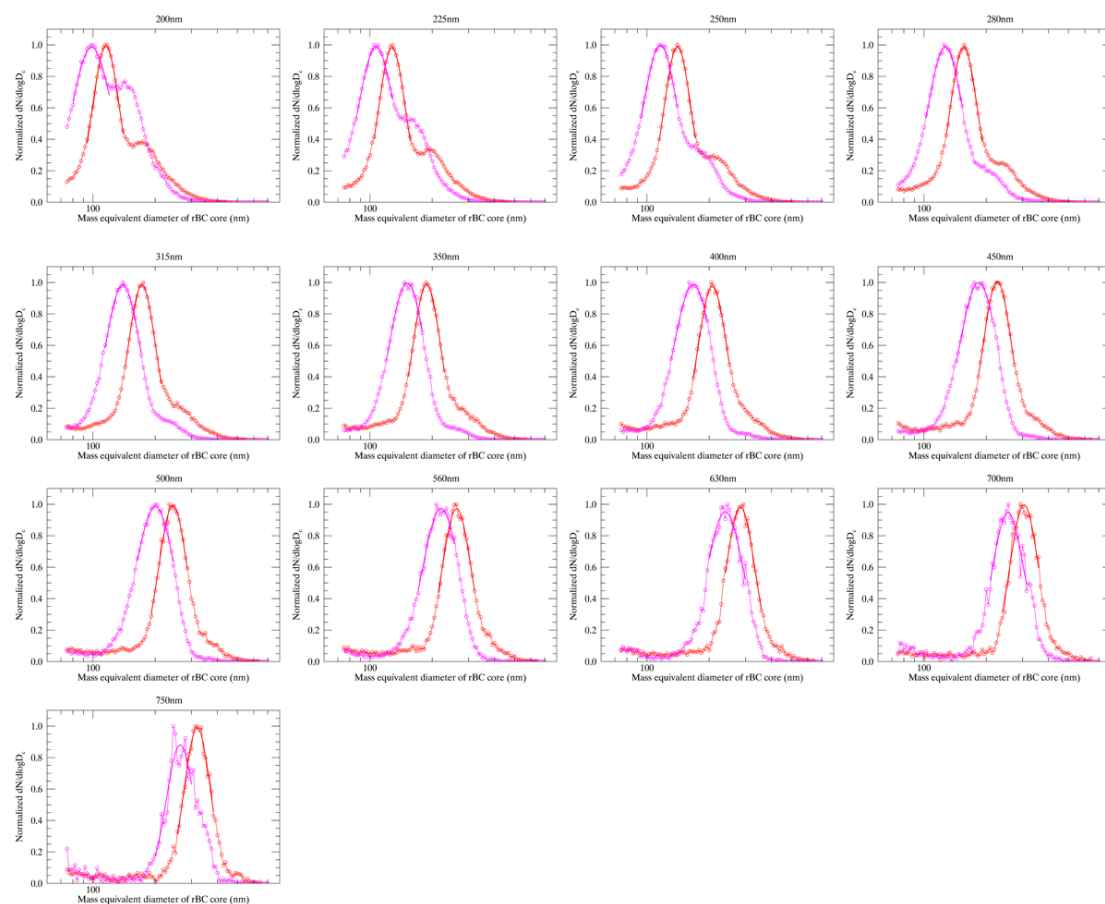


**Fig. R2** Normalized number size distributions of the rBC core in extBC (red) and thickly coated BC particles (magenta)

On this topic two important related points should be made. Thick coatings are more likely to be acquired by smaller particles (Fierce et al., 2016). And it is possible that core-shell coatings are more likely for larger particles (Liu et al., 2017).

**Reply:** We have read the two suggested references carefully. However, only the extBC aggregates without coating and a possible fraction of thinly coated BC aggregates are concerned in current study. The size-resolved mixing state of BC-containing particles will be discussed in our future study. In the revision, rough mixing states of size-resolved BC particles, calculated as the ratios of number concentration of extBC particles to the sum of extBC and intBC particles, at different mobility sizes are presented as shown in Fig. S9. Note that effects of multicharged particles are not eliminated. However, the multicharged particles should result in a similar effect on extBC and intBC at a given mobility. Thus, they should influence little of the number fraction of extBC in the total BC-containing particles. Size distribution of number fraction of extBC is used to auxiliary interpret the possible mechanism of the relatively higher masses and effective densities of extBC in the  $d_{\text{mob}}$  range of 280–350 nm in the revision (Lines 566–591).

## 2. Interpretation of the 'effective density' and 'fractal dimension'

The first major comment makes it clear that the 'effective density' and 'fractal dimension' results are biased towards fresh soot particles. In addition to this bias, the 'effective density' is a quantity which should correspond to the apparent density of a sphere with diameter equal to  $D_m$ . When using the DMA-SP2 setup employed in this study, the 'effective density' has virtually no meaning, since coatings are not measured by the SP2 as rBC. I do not see how this quantity could be useful for any future studies. If the authors wish to report such a quantity, they must explain in what context it should be interpreted. It should not be called 'effective density', which will confuse readers. The quantity called 'fractal dimension' has the same problem as the 'effective density.' In addition, the quantity should have been called 'mass-mobility exponent' (Sorensen, *Aerosol Sci Technol*, 45:765-779, 2011, doi:10.1080/02786826.2011.560909). It may be more interesting to compare the mixing state retrieved by asking 'is this particle similar to fresh soot?' (according to the 'effective density') with the mixing state retrieved by SP2 coating thickness analysis. But the usefulness of such an analysis is not guaranteed, the uncertainties may be too large.

**Reply:** Thanks for the professional comments. As presented in the original manuscript,

the effective density and fractal dimension of externally mixed BC (extBC) were analyzed instead of the entire BC-containing particles. The morphology and effective density of thickly coated BC particles were not discussed in our study. They have been studied in the previous literature, e.g., Zhang et al. (2016), using the SP2 and VTDMA measurements. In our study, the extBC particles are identified according to the time-delay between the incandescence signal peak and the scattering signal peak measured by the SP2. Only the BC-containing particles with delay times less than the criterions (2.0  $\mu\text{s}$  or even lower) are considered extBC particles. The remaining BC-containing particles are considered thickly coated by nonrefractory components. As mentioned in our responses to the first major comment, a fraction of thinly coated BC particles might also be considered the extBC particles based on the time-delay approach. These thinly coated BC particles should influence the shape of the frequency or size distribution but have few impacts on the determined typical mass or mass-equivalent diameter of the extBC. Thus, we propose that the results presented in our current manuscript should be reliable.

Actually, the thickness of the BC-containing particle can be retrieved using a specific approach, i.e., lead-edge-only (LEO) fitting (Gao et al., 2007). The method can estimate the optical size of particles using the scattering signal detected by SP2 at the beginning stage (e.g., the first 5%) by assuming certain parameters, including the refraction indices of coating materials and the rBC core. Compared to the size of the rBC core determined using the incandescence signal, the thickness of the coating can be estimated. However, this approach needs the scattering signal measured by the split channel of the SP2 (a two-element APD). The scattering signal detected by this channel is used to determine the center location of the Gaussian-distributed laser beam. Unfortunately, this channel of our SP2 was out of work during the experiment. We failed to use this method to estimate the coating thickness of individual BC-containing particle in the present study. However, the ‘coating thickness’ is not a crucial quantity in our current study. Only the extBC particles without or possibly with thin coating are investigated. Moreover, because a number of assumptions are employed in the LEO fitting, large uncertainties also exist in the retrieved coating thickness. Similar statements have presented in our revised manuscript as shown from Line 248 to 267.

Since only the extBC particles are analyzed, the ‘effective density’ and ‘fractal dimension’ should have practical meanings. Actually, the ‘fractal dimension’ we defined on the basis of the mass-mobility relationship of extBC is the ‘mass-mobility scaling exponent’. It is different from the virtual ‘fractal dimension’ of BC aggregates (Sorensen, 2011), while also represents the morphology of BC aggregates. Although the ‘effective density’ and ‘mass-mobility scaling exponent’ of fresh soot particles were

measured using a range of methods, the DMA-SP2 method was seldom used, especially in the ambient atmosphere. The advantage of the DMA-SP2 method is that the SP2 can distinguish the extBC from the thickly coated BC particles at the same time as measuring the masses of their rBC core, allowing to obtain the mass-mobility relationship in different atmospheric environments. While previous studies using the DMA-APM-CPC method were mainly conducted in the laboratory or in the source environments (e.g., in the tunnel). Meanwhile, the DMA-APM-CPC generally measured the mobility size not exceeding 350 nm in  $d_{\text{mob}}$  due to the very number concentrations of soot particles at larger particle sizes with the  $d_{\text{mob}} > 350$  nm. The SP2 measures the particle-to-particle rBC mass, thus has a higher efficiency in the detection of larger BC-containing particles. The stepwise measurement of DMA-SP2 also provide a high time-resolution of the ‘effective density’ and ‘mass-mobility scaling exponent’ at different mobility size, which can be used to study the variation of these quantities and the possible reasons. Similar statements are presented in the last paragraph of the introduction in the revision.

In addition, we find that the effective densities of size-resolved extBC obtained from the DMA-SP2 measurement are slightly lower than those determined using the DMA-APM-CPC method. Although we have given reasonable interpretation to the difference in our manuscript, further measurements are needed to examine the difference between the two tandem methods, e.g., by measuring diesel exhaust particles synchronously.

The uncertainty of the mass determination of extBC is estimated to be ~20% at each  $d_{\text{mob}}$ , including the uncertainty (~10%) in the rBC mass which is converted from the incandescence peak height measured by the SP2 and the uncertainty (~10%) arisen from the discrimination of extBC by using different delay time criterions. We have added similar discussion on the measurement uncertainties in the revision (Lines 277–283, 371–376).

Minor comments:

1. It was not clear to me why the points in Figure S2 were quantized. Why does the number concentration nto vary smoothly?

**Reply:** Figure S2 (Fig. S1 in the revised supplemental file) showed an example of the number concentrations of particles (including scattering and incandescence ones) detected by SP2 during a short circle and a long one. The operated flow rate of the SP2 was set to 100 cc per minute during this experiment. The smooth number concentration is related to the quite low number concentration of the size-selected particles.

2. In the abstract: effective density is not morphology.

**Reply:** We have modified. We have checked throughout our manuscript to make the expression more rigorous. Moreover, we have written the abstract of the revised manuscript.

3. The discrepancy between DMA-APM and DMA-SP2 measurements cannot be explained by the SP2 only being sensitive to rBC. The SP2 is calibrated using an APM (or CPMA). The former DMA-APM studies used denuded soot. The discrepancy is due to the limitations of the SP2 calibration.

**Reply:** We calibrated our SP2 using the size-resolved Aquadag particles selected by the DMA as mentioned in the section 2.3 of our revision manuscript. The effective densities of mobility size -selected Aquadag particles were referred to Gysel. (2011). Calibrations were well conducted before and after the experiment. As shown in Fig. S3 in the revised supplemental file, the calibration curve obtained after the campaign is consistent to that obtained before the campaign (with difference in the calibration factor < 3%). Even when the denuded soot particles are measured, there also remain a possibly small fraction of non-BC components which can be measured by the APM but cannot be determined by the SP2. Rissler et al. (2014) revealed that the residual mass fraction of volatile and/or semivolatile materials in the soot aggregate was ~10% even when the sample air was heated to 300 °C before entering the system for measurement.

4. Line 55 – Thick and thinly coated needs to be defined. The authors may find that in fact most atmospheric BC is coated.

**Reply:** We used the time-delay method to distinguish the mixing state of refractory BC (rBC). Two type rBC-containing particles can be distinguished. One is the rBC thickly coated by nonrefractory components and the other is rBC thinly coated or without coating (bared). The thickness of the coatings cannot be accurately identified in current study. As mentioned in the introduction of the manuscript, there also be a considerable fraction of extBC in the atmosphere especially in the urban regions (Lines 77–82 in the revision). The extBC discriminated using the time-delay method accounted for even >50% of the total BC-containing particles which were detectable by the SP2 in urban Beijing, although a fraction of extBC might be thinly or even moderately coated. The TEM analysis also showed that the bare-like soot particles accounted for 25% of the total soot particles in urban, and as high as 64% in tunnel. 63% soot particles were partly coated in urban environment (Wang et al., 2017). Thus, the morphology and effective density of these extBC aggregates in the atmosphere are studied.

Actually, the thickness of the coat can be retrieved from the scattering signals of the SP2 using the lead-edge-only (LEO) fitting (Gao et al., 2007). However, the notch in

the two-element APD of our SP2 failed to fix in an adequate position in this experiment. Thus, the optical size and the consequent coating thickness of the BC-containing particles cannot be estimated in current study. However, the coating thickness is not a crucial quantity in our current study on the morphology and density of uncoated BC aggregates. It can provide a validation of our discrimination of *ext*BC but should have little influence on our final analysis and discussion presented in the current study. Similar statements are presented in Lines 248–267 in our revised manuscript.

5. Line 88 – explain the reasons for the detection limits.

**Reply:** As mentioned in Lines 111–123 in the revision, larger uncertainties exist in the DMA-APM-CPC measurement for larger particles (e.g., with a  $d_{\text{mob}} > 350$  nm) which are much less abundant in the atmosphere than the smaller particles. Thus, the previous tandem measurements generally provided the mass-mobility relationship of BC aggregates with a  $d_{\text{mob}}$  not exceeding 350 nm.

6. Line 110 – quasi-monodisperse needs to be quantified or specified precisely. AMT is a technical journal.

**Reply:** Due to the effect of DMA transfer function, particles within a certain  $d_{\text{mob}}$  range are selected by the DMA at a given voltage. Usually, the particle number presents a triangle distribution as the function of  $d_{\text{mob}}$  at a given voltage. The peak of the triangle distribution corresponds to the certain  $d_{\text{mob}}$  which we are used in this study. A slight modification to the statement is performed in the revision (Line 184). In the current manuscript, we won't specify the principle of DMA that used to quantify the quasi-monodisperse since it is out of our current research scope.

7. Line 149 specify the intensity of the laser in units of W/m<sup>2</sup> or similar

**Reply:** Usually, the intensity of the laser is not specified in the SP2 study. Although the intensity of laser would influence the detection efficiency of SP2, it is usually checked indirectly by using the monodisperse Polystyrene Latex (PSL) at a given size (e.g., 269 nm). The intensity of the laser depends on the laser current which can be set manually in the SP2 acquisition software.

After the experiment, we used the DMA-SP/CPC system to measure the bare BC (Aquadag) particles. The detection efficiency was obtained by comparing the particle number concentration detected by the SP2 to that measured by the CPC at each prescribed mobility, as shown in Fig. S4 in the revised supplement file. Adequate detection efficiencies (>~90%) of SP2 are found when the mass-equivalent diameter of rBC core is larger than ~90 nm.

8. Line 153 frequency is the wrong word.

**Reply:** We have changed the word 'frequency' to 'frequency distribution' in our revised manuscript (Line 234).

9. Line 185 define K.

**Reply:** Have defined in the revision (Line 405).

10. Line 255 discuss the Diffusion-Limited Cluster-Cluster Aggregation mechanism (see Sorensen citation above)

**Reply:** We have read the review literature (Sorensen, 2011) carefully and found that the mass-mobility scaling exponents measured using the tandem techniques (e.g., DMA-APM, DMA-SP2) were sometime erroneously equivalent to the virtual fractal dimension of BC aggregates. The same mistake occurs in our current study. Corrections to this mistake have been performed in the revision (e.g., Lines 87–107, 393–396).

11. Line 261 organics do not 'fill in the gap', they cause restructuring

**Reply:** Corrected in the revision (Lines 432–434)

12. Line 357 the drag force, or uncertainty? Figure 6 needs error bars. Counting statistics will be poorer at the extreme sizes, possibly causing the observed trend.

**Reply:** We have rewritten Section 4.3 as shown in Lines 601–613 in the revision. A more reasonable interception is presented for the hiatus in the increase trend of dynamic shape factor.

## References

- Gao, R. S., Schwarz, J. P., Kelly, K. K., Fahey, D. W., Watts, L. A., Thompson, T. L., Spackman, J. R., Slowik, J. G., Cross, E. S., Han, J.-H., Davidovits, P., Onasch, T. B., and Worsnop, D. R.: A novel method for estimating light-scattering properties of soot aerosols using a modified single-particle soot photometer, *Aerosol Sci. Technol.*, 41, 125–135, doi:10.1080/02786820601118398, 2007.
- Gysel, M., Laborde, M., Olfert, J. S., Subramanian, R., and Gröhn, A. J.: Effective density of Aquadag and fullerene soot black carbon reference materials used for SP2 calibration, *Atmos. Meas. Tech.*, 4, 2851–2858, doi:10.5194/amt-4-2851-2011, 2011.
- Gysel, M., Laborde, M., Mensah, A. A., Corbin, J. C., Keller, A., Kim, J., Petzold, A., and Sierau, B.: Technical Note: The single particle soot photometer fails to reliably detect PALAS soot nanoparticles, *Atmos. Meas. Tech.*, 5, 3099–3107, doi: 10.5194/amt-5-3099-2012, 2012.
- Laborde, M., Mertes, P., Zieger, P., Dommen, J., Baltensperger, U., and Gysel, M.: Sensitivity of the Single Particle

- Soot Photometer to different black carbon types, *Atmos. Meas. Tech.*, **5**, 1031–1043, doi:10.5194/amt-5-1031-2012, 2012.
- Park, K., Cao, F., Kittelson, D. B., and McMurry, P. H.: Relationship between particle mass and mobility for diesel exhaust particles, *Environ. Sci. Technol.*, **37**, 577–583, doi:10.1021/es025960v, 2003.
- Raatikainen, T., Brus, D., Hooda, R. K., Hyvärinen, A.-P., Asmi, E., Sharma, V. P., Arola, A., and Lihavainen, H.: Size-selected black carbon mass distributions and mixing state in polluted and clean environments of northern India, *Atmos. Chem. Phys.*, **17**, 371–383, doi:10.5194/acp-17-371-2017, 2017.
- Rissler, J., Nordin, E. Z., Eriksson, A. C., Nilsson, P. T., Frosch, M., Sporre, M. K., Wierzbicka, A., Svenningsson, B., Löndahl, J., Messing, M. E., Sjogren, S., Hemmingsen, J. G., Loft, S., Pagels, J. H., and Swietlicki, E.: Effective density and mixing state of aerosol particles in a near-traffic urban environment, *Environ. Sci. Technol.*, **48**, 6300–6308, doi:10.1021/es5000353, 2014.
- Sorensen, C. M.: The mobility of fractal aggregates: A review, *Aerosol Sci. Technol.*, **45**, 765–779, doi:10.1080/02786826.2011.560909, 2011.
- Wang, Y. Y., Liu, F. S., He, C. L., Bi, L., Cheng, T. H., Wang, Z. L., Zhang, H., Zhang, X. Y., Shi, Z. B., and Li, W. J.: Fractal dimensions and mixing structures of soot particles during atmospheric processing, *Environ. Sci. Technol. Lett.*, **4**, 487–493, doi:10.1021/acs.estlett.7b00418, 2017.
- Zhang, Y. X., Zhang, Q., Cheng, Y. F., Su, H., Kecorius, S., Wang, Z. B., Wu, Z. J., Hu, M., Zhu, T., Wiedensohler, A., and He, K. B.: Measuring the morphology and density of internally mixed black carbon with SP2 and VTDMA: new insight into the absorption enhancement of black carbon in the atmosphere, *Atmos. Meas. Tech.*, **9**, 1833–1843, doi:10.5194/amt-9-1833-2016, 2016.

## Response to reviewer#2

### General comments

The authors use a tandem DMA-SP2 system to measure the mass-mobility exponent, effective density, and shape factor of ambient BC particles in Beijing, China. Despite the claim to novelty made in the title similar combined DMA-SP2 measurements have already been discussed and reported in the literature, which the authors have failed to discuss. In addition, there are significant shortcomings in the manuscript itself, ranging from inadequate description of the experimental details and results to data quality issues. In my view the manuscript is at the 'early draft' stage rather than the 'under review' stage. I believe major revisions are required before the manuscript can be considered for publication in AMT. Most importantly, the authors need to better demonstrate why this study is an original contribution to the literature on the properties of ambient BC aerosols, and why their measurements should be considered artifact-free and trustworthy.

We appreciate the criticisms from the reviewer and appreciate the several useful comments which helped us improve the paper. A huge modification has performed to our manuscript by referring more useful literature, reanalyzing the experimental data and improving the English writing. We hope the reviewer will see our efforts to improve the quality of our manuscript.

I see the following major issues:

The study is not placed in appropriate context through citation of relevant literature. In the title and elsewhere (e.g. L101) the authors claim that this is a 'novel' system or measuring the morphology and effective density of black carbon particles. This is incorrect. Tandem DMA-SP2 measurements have been discussed and/or performed in a number of different studies (e.g. Gysel et al., 2011; Raatikainen et al., 2017; Zhang et al., 2016). A handful of references are cited for more general mass-mobility measurements (e.g. using an APM rather than an SP2). But the literature on this topic is more extensive than this small selection of studies would suggest, including a review on the mobility of fractal aggregates by Sorensen (2011). I suggest the authors read this review and the references therein and put more effort into placing their measurements into the context of these previous works. In particular, the authors need to demonstrate what is the original contribution of this work.

**Reply:** Thanks for the constructive comments. Indeed, a number of previous studies have used the tandem DMA-SP2 system to measure the physical and/or optical

properties of BC particles. A few related references have been cited in the initial manuscript (e.g., Gysel et al., 2011; Zhang et al., 2016), although a few other references were missed (e.g., Raatikainen et al., 2017). Citation of these related references has been performed in our revised manuscript. As mentioned in the introduction of the revision (Lines 129–141), the mass-mobility relationship, from which the morphology and effective density of extBC aggregates are obtained, were seldom studied in previous DMA-SP2 measurements, especially in the ambient atmosphere. The morphology and effective density of internally mixed BC (intBC) particles in the atmosphere in North China Plain were studied by using the VTDMA-SP2 measurement (Zhang et al., 2016). We should not miss the valuable review literature (Sorensen, 2011) in our initial manuscript. We have read the literature carefully according to the reviewer's comment and found that the 'mass-mobility scaling exponent' was erroneously considered the virtual 'fractal dimension' even they have a corresponding relationship and both reflect the morphology of BC aggregates. Similar mistakes also existed in previous studies on mass-mobility relationship (e.g., Park et al., 2003). Corrections can be found in Lines 87–107, 393–396 in the revision. By carefully referring to this review article, we have improved our understanding in the subject of the morphology of BC aggregates. Then we further condense our research purpose as shown in the rewritten introduction of the revision. As presented there, although the morphology and effective density of BC aggregates have been widely studied using the TEM analysis and/or tandem techniques (e.g., DMA-APM), such studies were mainly conducted in the laboratory and/or in the source environments (e.g., in the tunnel) where the freshly emitted soot aggregates were predominant. The SP2 provides an advantage to distinguish the extBC aggregates from the thickly coated BC particles at the same time to the rBC mass determination. Thus, the DMA-SP2 can be deployed to different atmospheric environments to investigate the mass-mobility relationship of ambient extBC. Another advantage of the DMA-SP2 tandem system is that it can investigate the mass-mobility relationship of BC aggregates in a relatively larger mobility range (e.g., in the 350–750 nm mobility diameter range) due to the high sensitivity and accuracy of the SP2 in the rBC mass determination in this range, allowing to examine the applicability of the mass-mobility relationship obtained from previous studies and the consistence of the mass-mobility relationship determined using different tandem techniques. Previous DMA-APM measurements seldom concerned the BC aggregates in the atmosphere with mobility diameter ( $d_{\text{mob}}$ ) larger than 350 nm due to the larger measurement uncertainty in the larger particle sizes. Thus, our study should have its practical and scientific meaning, even the DMA-SP2 tandem technique is not novel. We have removed the word 'novel' in the title of our manuscript according to the reviewer's comment.

The quality of the writing is not at a suitable level for scientific publication. There are many English grammar issues - too many to list in a scientific review. Beyond this, the language is frequently too vague. To take just the first example I come across the authors state that BC can lead to 'Earth warming' on L39. I believe that authors mean 'warming of the Earth's atmosphere' or similar. There are many more examples of such lazy language throughout the manuscript.

**Reply:** Thanks for the professional comments. Actually, the writing of our manuscript had been polished by native English speakers before it was submitted to the journal for review. They might have made an improvement in the English grammar and writing. A number of more professional contents (e.g., the example posed by the reviewer) are still needed to improve. We checked carefully throughout our manuscript to make corrections to these similar mistakes. The revised manuscript has been further polished by a more professional agency before resubmitted for review. We hope you can see the improvement in the English writing of our revised manuscript. Besides, we also have made efforts to improve the scientific quality of this article by rewriting a large fraction of the manuscript.

The study design and experimental and analytical details are inadequately described, which makes it difficult to judge their suitability. For example from what I can gather, the results presented in Figs. 2 to 6 are only for rBC-containing particles that displayed a delay time of less than 2 $\mu$ s (defined as 'extBC'). This needs to be clarified and stated more explicitly (another example of lazy language). The suitability of using delay time to distinguish between externally and internally mixed BC particles then requires further discussion. It is not as simplistic as the authors make it out to be. The authors allude to the fact that thinly-coated BC will exhibit low SP2 delay times on L280. This is also true for moderately-coated BC (e.g. with BC volume fractions as low as 30%), which would certainly not be classified as 'externally mixed' (ExtBC). A better approach for classifying BC mixing state with the SP2 is the quantitative LEO-fit approach (Gao et al., 2007; Laborde et al., 2012). The authors need to at least discuss this more sophisticated method, the reasons why they chose to use the more simplistic delay time approach, and the consequences of this decision.

**Reply:** The manuscript is written to discuss the physical properties (mainly the mass-mobility relationship) of externally mixed BC (extBC) particles, although the experiment was designed for a range of research aims. For example, the experiment was originally designed to also study the mixing states (e.g., the fraction of thickly-coated BC particles and the coating thickness) and optical absorption properties (e.g.,

mass absorption efficiency) of size-selected BC particles, and the number/mass size distribution of BC particles in the atmosphere, similar to the experimental setup presented in Raatikainen et al. (2017). Two micro-aethalometers used to determine the aerosol absorption coefficients were also connected to the DMA and measured parallel with the SP2 (as shown in Fig.1 in the manuscript). The data analysis is still in progress. Several difficult but crucial issues should be deal with in data processing, e.g., the effects of multi-charged particles. At the current stage, we present our first study on the mass-mobility relationship of the extBC particles, although the effects of multicharged particles are also needed to take into consideration. A number of the technical details associated with this experiment are described in current manuscript. Further studies mentioned above are also in preparation. Similar statements are also presented in the revised Section 2 (Lines 201–206).

In this study, the extBC particles are discriminated according to the delay time between peaks of the incandescence signal and the scattering signal measured by the SP2. Only the BC-containing particles with the delay times less than the criterion are recognized as the extBC particles. The remaining BC-containing particles were considered thickly coated by non-refractory components. The criterion is determined from the frequency distribution of delay time of individual particles. As shown in Fig. S1, the frequency distribution of delay time exhibits a significantly bimodal pattern. The delay time corresponding to the minimum of the frequency distribution between the bimodal peaks is chosen as the criterion. In this study, the criterion of the time delay is selected as 2.0  $\mu\text{s}$ . Indeed, a fraction of thinly coated BC particles might be also recognized as the extBC based on the time-delay approach. A few moderately coated BC particles (e.g. with BC volume fractions as low as 30%) might also have delay times less than the criterion as mentioned by the review (Laborde et al., 2012), which might be mistakenly recognized as the extBC. To examine the stability and reliability of our results derived by using the time delay approach, we strengthen the discrimination of mixing state by decreasing the criterions of delay time from 2  $\mu\text{s}$  to 1.2  $\mu\text{s}$  and 0.4  $\mu\text{s}$ . Reducing the delay times to less than 0.4  $\mu\text{s}$  means that the incandescence signal has the same peak location to the scattering signal because the minimum unit for the signal record is 0.4  $\mu\text{s}$ . The effects of thinly and even moderately coated BC particles are expected to decrease when the delay time threshold decreased from 2.0  $\mu\text{s}$  to 1.2  $\mu\text{s}$ , and then to 0.4  $\mu\text{s}$ . However, as shown in Fig. S5 (the frequency distributions of mass-equivalent diameter of rBC core ( $d_{\text{me}}$ ) of the extBC particles, which is calculated from the measured rBC mass by assuming the rBC core is a void-free sphere with 1.8  $\text{g cm}^{-3}$  density, at the prescribed mobility size ranges) and Fig. S6 (the normalized number size distribution of rBC core of the extBC particles) in the revised supplemental file, the

decrease in the delay time threshold has insignificant impacts on the peak location of frequency or number size distribution, i.e., the typical  $d_{me}$  of extBC at each prescribed mobility size, although the data volume used to calculate the distribution reduced significantly. As also shown in Table S1, the discrepancy in the fitted peak  $d_{me}$  values resulting from the different delay time thresholds don't exceed 3% in the current study. It means the differences in fitting peak values of rBC mass don't exceed 10%, which is considered as the uncertainty in the determined rBC mass at each mobility size due to the time-delay method employed to distinguish the extBC particles from the thickly coated BC particles. The thinly coated and even moderately coated BC particles mistakenly considered as the extBC discriminated by using the time-delay method appear to influence the shape of the size distribution. These particles mixed with multicharged extBC particles resulting in an increase in the size distribution at its right tail. At the current stage, we are unable to separate which particles presented in the right tail are thinly/moderately coated and which are multicharged. However, this issue should affect little on the results presented in our current study. Similar statements are also presented in the revised Section 3.2 (Lines 344–379 in the revision).

Actually, the thickness of a BC-containing particle can be retrieved using a specific approach, i.e., lead-edge-only (LEO) fitting (Gao et al., 2007). The method can be used to estimate the optical size of the particle using the scattering signal detected by SP2 at its initial stage (e.g., the first 5%) by assuming certain parameters, including the refraction indices of coating material and the rBC core. By comparing with the mass-equivalent diameter of the rBC core determined by using the incandescence signal, the thickness of the coating can be estimated. However, this approach needs the scattering signal measured by the split channel (with a two-element APD) of the SP2, which is used to determine the center location of the Gaussian-distributed laser beam. Unfortunately, this channel of our SP2 was out of work during the experiment. We failed to use this method to estimate the coating thickness of the BC-containing particle in the present study. However, the 'coating thickness' is not a crucial quantity in our current study because only the extBC particles without coating or with thin coating were concerned. The 'coating thickness' can be used to verify the results currently presented. Similar statements can also be found in the revised Section 2.3 (Lines 248–267 in the revision)

We are also preparing a new experiment which is similar to the presented one by employing a SP2 with all detect channels well performed. Moreover, because a number of assumptions are employed in the LEO fitting and the subsequent Mie calculation, large uncertainties are also exist in the retrieved coating thickness. For instant, the size of the rBC core ( $d_{me}$ ) is determined from the rBC mass (calculated according to the

linear relationship between incandescence single peak and rBC mass calibrated before and after the experiment) by assuming it is a void-free sphere with  $1.8 \text{ g cm}^{-3}$  density. If the BC particle is not void-free and has a low density (Zhang et al., 2016), the size of the rBC core might be underestimated. In addition, the optical size of the particle largely depends on the refraction indices of the coating materials and the rBC core, which are usually known for a specific site. Generally, the coating thickness is not a crucial quantity in our current study of the morphology and density of uncoated extBC aggregates. It can provide a validation of our discrimination of extBC but should have little influence on our final analysis and discussions presented in current study.

The material as presented gives cause to question the quality of the measurement data, but insufficient details are provided to fully make this assessment. Specific points are highlighted below in relation to Fig. 2, which contains features that require explanation (absence of clearly defined peaks for multiply charged particles, presence of peaks with rBC mass approaching 0). In addition for reasons that are not yet satisfactorily explained, the effective density results presented in Fig. 5 are systematically lower than previous measurements (both the previous studies already cited by the authors as well as previous DMA-SP2 measurements that were also conducted in Beijing but are not yet discussed; Zhang et al., 2016). Given these issues, the authors should include further data and explanations to build confidence in their results and to confirm that the measurements are artifact-free. For example, were PSL spheres or other monodisperse particles (e.g. aquadag for the SP2 measurements) used to confirm that the DMA was operating correctly? What quality checks were performed to ensure the SP2 was operating correctly? (E.g. laser and detector block properly aligned, laser power levels, flow rate checks, comparison of calibration curves with previous calibration curves of the instrument).

**Reply:** Thanks for the comments, we have increased the description in the detail of the experiment and data processing in the revision. Meanwhile, we used the number size distribution of rBC core of the extBC particles in the revision instead of the initial frequency distribution of rBC mass of the extBC particles. The normalized number size distribution is a more practical quantity in the scientific research and has lower artificial uncertainties than the frequency distribution which depends on the bin-size used to calculate the frequency. We have completely reanalyzed our dataset and present more reliable results in the revision. Discussions on the measurement uncertainty are also presented. Specific responses to the review's queries are presented point-to-point below.

- (1) Peaks with rBC mass approaching 0 presented in the frequency distribution of rBC mass are likely attributed to the measurement noises of the SP2. Explicit discussions

are also presented in the response to the No.18 specific comment. The smaller rBC masses approaching 0 were also observed in the SP2's incandescence calibration using size-selected Aquadag particles (Fig. R1). As shown in Table R1, the number contribution of measurement noises gradually increases from 1% at 140 nm  $d_{mob}$  to 37% at 750 nm  $d_{mob}$ . The noises should be resulted from the SP2 measurement only and not presented in the CPC measurement. As shown in Fig. R2, if the noises are not eliminated, the counting efficiency of SP2 (calculated as the ratio of number concentration measured by the SP2 to that counted by the CPC at a given mobility) shows an increase trend with increasing  $d_{mob}$ . While after correction to the effect of these noises, the counting efficiency of SP2 is stably close to 100% in the 125–750 nm  $d_{mob}$  range. We have used the normalized number size distribution of rBC core of the extBC particles instead of the initial mass frequency distribution. The effect of these small rBC masses on the number size distribution is significantly reduced due to data processing.

As also shown in Fig. R1 and Table R1, the doubly charged particles shown a discernable minor peak in the frequency distribution of the incandescent peak height in the calibration using Aquadag particles. Since the Aquadag particles generated from the aerosol generator can be considered as the bare BC, the mobility of Aquadag particles should be only related to their masses and morphologies, resulting in the clear peak of multicharged particles. However, in the ambient atmosphere, it is more complex even for the extBC particles. As mentioned above, a fraction of thinly coated particles is also recognized as extBC based on the time-delay discrimination. These particles coexisted with the multicharged particles result in a combined effect on the size distribution of rBC core of the extBC particles at a given mobility. They mainly result in an increase in the size distribution at its right tail and have few effects on the determined typical  $d_{me}$  of extBC. Similar statements can be found in Lines 344–379 in the revision. Anyway, based on the clear distinguishable minor peak presented in the frequency distribution of the incandescence peak height for the multicharged bare BC particles (Aquadag particles) and the adequate detection efficiency of SP2, we propose the DMA-SP2 system operated normally in this experiment.

- (2) The observation data have been reanalyzed. The effective densities of extBC obtained from the recalculated mass-mobility relationship at the prescribed mobility sizes are slightly lower than those obtained from the previous DMA-APM measurements. The deviations are general in the measurement uncertainty of DMA-SP2 system (~20%). The slightly lower densities of extBC aggregates are also likely due to the differences in the mass determination between APM and SP2. The APM

measures the mass of whole BC aggregate, which might be composed of a fraction volatile or semivolatile materials in addition to the primary BC spherules. While the mass of rBC is determined by using the SP2. Thus, a slightly lower mass of extBC aggregates can be expected at a given mobility size. Meanwhile, the volatile and/or semivolatile materials might also result in a more compact structure of extBC aggregate due to the reconstruction effect by these materials thinly coated outside the primary BC particles. The extBC mass determined as the peak rBC mass of the size distribution of rBC core of the extBC particles might mostly correspond to the uncoated extBC which are less influenced by the volatile and/or semivolatile materials. It also results in the slightly lower densities obtained from the DMA-SP2 measurement than those from previous DMA-APM measurements. Anyway, the densities derived from the reanalyzed dataset are generally comparable to previous values for diesel soot particles in the laboratory and in the source environments such as in the tunnel.

The effective densities of thickly coated (internally mixed) BC (In-BC for short in the reference) particles were presented in Zhang et al. (2016). Due to the significant reconstruction by the nonrefractory components thickly coated outside the primary BC particles, these BC particles became more compact resulting in obviously higher effective densities than the uncoated BC aggregates presented in current study.

- (3) Before this experiment, the laser alignment was performed by the operator according to the manual provided by manufacturer step-by-step. Besides the incandescence calibration using Aquadag particles, the scattering calibration using PSL with a certain diameter (269 nm) were also carried out before and after the campaign. A slight decrease in the measured scattering peak height (low-gain) for 269 nm PSL was observed after the campaign compared to that before the campaign (from 3576 to 3555 a.d.). It indicates the laser of the SP2 was stable throughout the campaign. Since the split channel was out of work in the experiment, the absolute value of the scattering peak height for 269 nm PSL appears to be useless in this study, which is mainly used in the retrieval of particle optical size by using the LEO fitting method. In the scattering calibration of the SP2, we also delivered the 269 nm PSL to pass through the DMA before to be measured by the SP2. We examined the SP2 recorded particle number concentrations by adjusting the mobility diameters of particles through the DMA. Because the PSL particles are general spheres, their mobility diameters are equal to their geometric diameter. Thus, we found that the recorded number concentration showed a significant peak when the mobility was set to ~269 nm for the 269 nm PSL in the calibration. It indicates the DMA was operated correctly although the number concentration was not recorded

in the compute.

Generally, the DMA-SP2 system was operating correctly in the experiment.

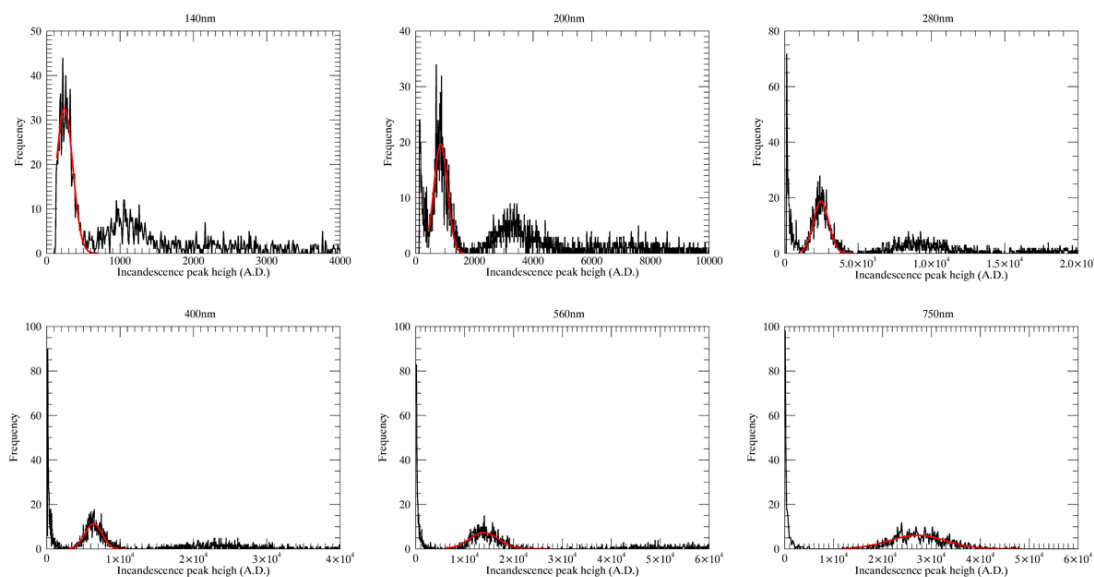


**Fig. R1** Frequency distributions of incandescence peak height detected by SP2 for size-selected Aquadag particles at the prescribed mobility sizes. The Gaussian fitting is performed for the major peak of each distribution to obtain the typical incandescence peak height at the corresponding mobility size.

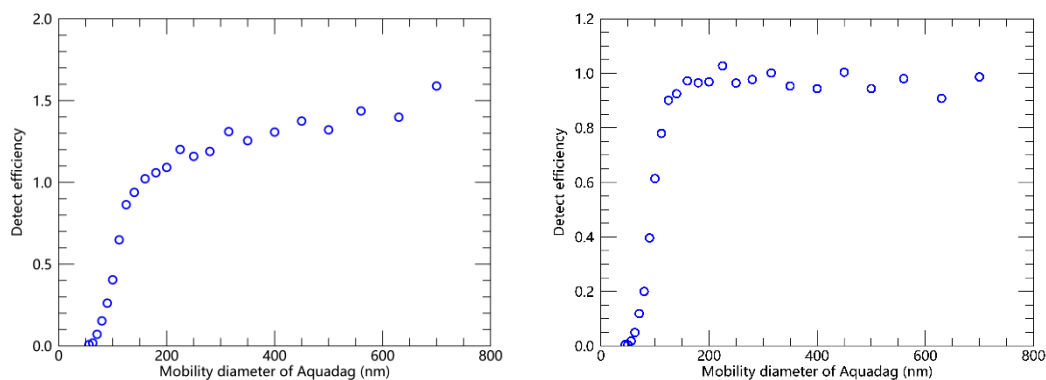


**Fig. R2** Detection efficiency of the SP2 to Aquadag particles with different mobility diameter in the range of 50–750 nm selected by the DMA. The left panel shows the detect efficiency of SP2 including the effect of measurement noises and the right is noise-corrected detection efficiency.

**Table R1** Number fractions of single charged particles, detection noises, and multiply charged particles at different mobility sizes in the measurement for Aquadag particles using the DMA-SP2 tandem system. As shown in Fig. R1, the high frequencies of incandescence signal peak height close to 0 are considered to be attributed to the detection noises. The major peak of the frequency

distribution is attributed to single charged Aquadag particles and the minor peak at the right side of the major one is considered to be resulted from double charged Aquadag particles.

Mobility Diameter	Single charged (%)	Noise (%)	Multi-charged (%)
140	47	1	52
160	45	4	51
180	39	7	54
200	37	9	54
225	37	13	50
250	39	14	47
280	40	16	44
315	41	21	38
350	43	21	36
400	47	25	28
450	50	25	25
500	54	26	20
560	56	29	15
630	64	33	3
700	62	37	1
750	71	29	0

No uncertainty estimates are provided for the measurements and main results. This is important as the SP2 counting statistics and therefore measurement errors will be sizedependent. How sensitive are the reported quantities (e.g. Df) to these measurement uncertainties?

**Reply:** Discussions on the uncertainty in the determination of extBC mass have been performed in the revised manuscript. The uncertainty in the typical extBC mass at each mobility is arisen mainly from two aspects. One is the uncertainty in the rBC mass measured by the SP2. It is mainly related to the uncertainty in SP2 incandescence measurement and the calibration factor that is determined from the rBC mass-incandescence relationship using the standard soot particles (Aquadag particles in this study). Approximately 3% variation in the calibration factor is estimated throughout the experiment. Both considering this deviation and the uncertainty in the measured incandescence signal and calibration material, we estimate the uncertainty in the measured rBC mass to be ~10%. The other uncertainty is arisen from the time-delay approach used to discriminate the extBC particles. By examining the effect of delay time threshold on the peak  $d_{me}$ , the associated uncertainty is estimated to not exceed 10%. Thus, the total uncertainty in the typical extBC mass used in the further mass-mobility relationship analysis is ~20%. Similar discussions can also be found in Lines 277–283, 371–376 in the revision.

The counting efficiency of SP2 is calculated as the ratio of particle number

concentration measured by the SP2 and that measured by the CPC at a given mobility selected by the DMA. The counting efficiency was examined using the Aquadag particles after the campaign. As shown in Fig. S4, the SP2 has adequate counting efficiencies (>90%) for Aquadag particles with mobility diameter ( $d_{\text{mob}}$ ) larger than 125 nm. The counting efficiency is stably close to 100% in the  $d_{\text{mob}}$  range of 125–750 nm. We converted the  $d_{\text{mob}}$  to mass-equivalent diameter ( $d_{\text{me}}$ ) of rBC according to the size-dependent effective densities of Aquadag particles (Gysel et al., 2011). The SP2 has adequate counting efficiencies (>90%) in the ~90–420 nm  $d_{\text{me}}$  range. Thus, the mass-mobility relationship of the extBC particles in 140–750 nm  $d_{\text{mob}}$  range presented in the current study should be reliable and has high confidence.

We propose the uncertainties in the determined extBC mass are similar at different mobility. It means if a lower (or higher) extBC mass is expected due to the uncertainty at a given mobility, the lower (or higher) extBC mass at other mobility sizes should also be expected. Although we don't discuss the sensitivity of mass-mobility scaling exponent to the measurement uncertainty in the manuscript, its sensitivity to the fitted size range is presented in the revision (Lines 450–457). Meanwhile, the deviation in the mass-mobility relationship in a polluted episode compared to that in a clean period also investigated (Lines 471–499 in the revision).

#### Specific comments

1. L69: 'Representativeness' instead of 'representation'

**Reply:** Thanks for the careful review. We have rewritten the introduction of our manuscript.

2. L80 - 82: The meaning of these sentences is not clear, rewording required

**Reply:** The initial purpose of the sentences is to express how the APM determines the mass of particles at a given mobility selected by the DMA. We have rewritten these sentences as shown in Lines 114–118 in the revision.

3. L92: Schwarz misspelt.

**Reply:** Have corrected in the revision (Line 129).

4. L98: Statement needs qualification. This is not true when measuring pure BC particles

**Reply:** We have rewritten the whole paragraph in the revision to highlight the practical significant and advantage of our study on morphology and effective density of ambient extBC in the atmosphere of urban Beijing using the DMA-SP2 tandem measurement

(Lines 124–172).

5. L109: Please include information about the neutralizer that was used upstream of the DMA. This is especially required when considering the potential impacts of multiply charged particles as discussed in Section 3.2.

**Reply:** A Kr neutralizer (model 3087, TSI Inc.) was utilized upstream of the DMA to charge the particles entering into the system. A simple description of the neutralizer has been added in the revised manuscript (Lines 185–186).

6. L135: Please include the length of the nafion dryer and the source of the dry sheath air.

**Reply:** A model MD-700-12F-3 (Perma Pure LLC, Toms River, NJ, USA) nafion dryer with length of 12 inch was used. The total sample flow rate passing through the nafion dryer was ~0.8 L/m. The dry sheath air was drawn by a Vacuum pump (KNF) opposite to the sample flow direction. We added these information in our revised manuscript (Lines 187–191).

7. L139: Some discussion is required about SP2 counting efficiency over this size range. It is not always 1, which will affect counting statistics, adding uncertainty to measurements reported at the limits of the range.

**Reply:** Although 33 mobility diameters was selected in each cycle, only the mobility diameters ( $d_{\text{mob}}$ ) in range of 140–750 nm are analyzed because the size distribution of rBC core of the extBC particles with a  $d_{\text{mob}}$  smaller than 140 nm cannot exhibit a clear peak, from which the typical mass-equivalent diameter ( $d_{\text{me}}$ ) of extBC is determined. The detection efficiency of SP2 is shown in Fig. S4 in the revised supplemental file by comparing the number concentration of generated Aquadag particles measured by the SP2 to that by the CPC at each mobility. As shown in Fig. S4, the SP2 has adequate detection efficiencies (>90%) for Aquadag particles with a  $d_{\text{mob}}$  not smaller than 125 nm, equivalent to a  $d_{\text{me}}$  larger than ~90 nm. Thus, the detection efficiency of SP2 should not have great effects in the 140–750 nm  $d_{\text{mob}}$  range we concerned in the current study. Since the peak  $d_{\text{me}}$  of the size distribution of extBC at each mobility is require, the low detection efficiency of SP2 to small particles should influence little of the results derived from our analysis.

8. L153: The phrase 'frequency of the time lag' does not make sense. I guess the authors meant frequency distribution or histogram.

**Reply:** Thanks. We used the 'frequency distribution' instead of 'frequency' in the

revision (Line 224).

9. L156: Am I correct in assuming that the 'extBC' results presented later only include particles that displayed a lag time less than 2  $\mu\text{s}$ ? If so please state this explicitly.

**Reply:** Yes, we only analyzed the mass-mobility relationship and effective density of 'extBC' distinguished according to the delay time between the incandescence peak and the scattering peak with lag times less than 2  $\mu\text{s}$ . Explicit statements are shown in Lines 230–247 in the revision.

Also including in the revision is the examination of the effect of delay time threshold (decrease from 2  $\mu\text{s}$  to 1.2  $\mu\text{s}$  and 0.4  $\mu\text{s}$ ) on the derived mass-mobility relationship of extBC. A decrease in the lag time threshold means a stricter discriminant criteria for the extBC particles using the time-delay method. It is discussed in detail in Section 3.2 of the revision.

10. L162: More sensitive than what? To Fullerene soot I presume but statements like this need to be explicit, avoiding lazy language.

**Reply:** The incandescence signal is more sensitive to Aquadag particles than to the Fullerene or diesel exhaust soot particles which are the mainly BC particles in the atmosphere, e.g., the same mass of Aquadag particle results in a high incandescence peak than the Fullerene soot or diesel exhaust soot. Similar corrections can be found in Lines 271–274 in the revision. We have check carefully throughout our manuscript to avoid similar writing errors.

11. L166: Please include a Figure in the supplementary information of the two measured incandescence calibration curves. Were the incandescence calibrations performed all the way up to 750 nm or were the calibration curves extrapolated? What sort of function was fit to the calibrations curves? Were the calibrations consistent with previous calibration curves measured for this instrument (an important check to make to ensure the SP2 was operating ok)

**Reply:** The calibration curves before and after the campaign are showed in the revised supplemental file (Fig. S3). In the two manually calibration for the incandescence signal of the SP2, Aquadag particles with the  $d_{\text{mob}}$  in the range of 100 nm to 450 nm (e.g., 100, 125, 150, 175, 200, 250, 300, 350, 400, 450 nm) was measured by the SP2. As shown in Fig. S3, the incandescence peak heights detected by the SP2 are linearly correlated with the rBC masses which are calculated according to the effective densities of Aquadag particles provided in Gysel et al. (2011). After the campaign, we also used the

DMA-SP2 tandem system to measure the generated Aquadag particles automatically. The setup of the DMA-SP2 system was the same as that used to measure the ambient particles. Thus, the relationship between the incandescence peak height and rBC mass obtained from the size-selected Aquadag in the  $d_{\text{mob}}$  range of 140–750 nm is established. As shown in Fig. S3, the linear relationship between the incandescence peak height and rBC mass is robust in the 100–750 nm  $d_{\text{mob}}$  range for our SP2. The calibration factors (the slopes of the linear regressions) vary little during this campaign, indicating the good performance of our SP2. The good performance of our SP2 can also be validated by the high detection efficiency (>90%) of our SP2 for BC particles with  $d_{\text{me}}$  larger than ~90 nm (Fig. S4).

12. L176: Please also discuss what the prefactor  $k$  represents (e.g. Sorensen 2011).

**Reply:** Since the mass-mobility relationship is studied, the prefactor  $k$  here is not consistent to that in the fractal relationship of DCLA aggregates presented in Sorensen (2011). The prefactor  $k$  (actually  $\log(k)$ ) is the intercept of the linear regression of extBC mass against its mobility diameter in the logarithm scale. The  $k$  value obtained in current study is in the same order of magnitude to the previous values for soot aggregates (Park et al., 2003). Explicit discussion can also be found in the response to the No.19 specific comment. Specific discussion on  $k$  will not be presented in the current manuscript.

13. L191: Please provide a reference for why this value of material density was chosen.

**Reply:** A reference, Taylor et al. (2015), is added in our revised manuscript (Line 411).

14. L199: The more common phrasing for this section would be 'Data processing'. And it seems to me that Section 2.4 would be a better fit in this section rather than the measurement methodology section above.

**Reply:** Thanks for the constructive comment. We have modified the title of Section 3 (Lines 286–287, Line 325) and moved the section 2.4 to 3.3 according to the suggestion.

15. L220: It seems that this method was not used in this study. Why is it mentioned? Was it used to check the results processed with the first method?

**Reply:** At the beginning of the experimental setup, we intended to use the correlation method. However, during the data analysis, we found that size distributions of SP2-detected particles were inadequate for the further calculation of the correlation coefficients since the detection efficiency of the SP2 decreases dramatically in the small particle range. Therefore, the local peak method is developed in current study to identify

the time difference between the size selection and the SP2 measurement. The correlation method will be used to examine the time difference between the size selection and the AE51/CPC measurements in our future study of the number and mass size distribution of BC. Similar statements are presented in the revision (Lines 317–323).

16. L232: 'Minimizing the multicharged particles' is too vague. Suggest 'Correcting for the presence of multiply-charged particles' or something similar.

**Reply:** Thanks. We adopt the suggestion of the reviewer by changing the title of Section 3.2 as 'Determination of the typical masses of extBC at prescribed mobility sizes'. We have also rewritten the whole content of this section to express explicitly how we determine the typical masses of extBC at prescribed mobility sizes. The effect of the delay time threshold chosen for the discrimination of extBC on the determined extBC masses is also discussed in the revision (Lines 326–379).

17. L240: Please be more specific. Exactly what parameter of the fitted curve was used to represent the mass of singly charged extBC particles?

**Reply:** In the initial manuscript, the mean value or expectation ( $\mu$ ) of the Gaussian distribution  $f(x) = A \exp(-\frac{(x-\mu)^2}{2\sigma^2})$  was used to represent the mass of singly charged extBC.

We use the number size distribution instead of the rough frequency distribution of rBC core mass of the extBC particles in the revision. The peak  $d_{me}$  determined as the mode value of the lognormal function fitted to the major peak of the number size distribution of extBC is considered the typical  $d_{me}$  of extBC (singly charged) at a given mobility. We have rewritten the whole content of Section 3.2 in the revision.

18. Fig. 2: These curves contain features that require discussion to build confidence in the measurements. For example: related to the comment above about L156, do these frequency distributions only contain particles that display time lag less than 2 $\mu$ s? If so, why are there sharp increases in the number of particles with rBC mass approaching 0 at diameters greater than 160nm? (With no filtering of the data applied I would assume these are heavily coated particles, which is a reason why I think the filtering process is not strict enough to be able to label these particles as 'extBC'). Why do the multiplycharged particles show up as a very fat tail that does not descend to a frequency of 0 until some point beyond the upper limit of the x-axis? What do these tails in the distribution represent? (E.g. they are in contrast

to what is typically seen in SP2 calibrations, when doubly and triply charged particles are observed as clear, separate gaussian peaks). I suggest adding vertical lines along the x-axis corresponding to the mass of particles selected by DMA (e.g. under the assumption of spherical particles with the material density of BC) to provide reference points to compare the measured mass distributions to.

**Reply:** The normalized number size distribution ( $dN/d\log D_c$ , where  $D_c$  is the mass-equivalent diameter of rBC core by assuming it is a void-free sphere with  $1.8 \text{ g cm}^{-3}$  density,  $N$  is the number concentration in a given  $D_c$  range) instead of the initially rough frequency distribution of extBC mass at each prescribed mobility in the range of 140-750 nm is presented in Fig. S6 in the revised supplemental file. Five normalized number size distributions at 140, 225, 350, 500, 750 nm  $d_{\text{mob}}$  are selected and also shown in Fig. 2 in the revision. The major peaks are more significantly through such data processing at prescribed mobility sizes. The size distributions of rBC core at different mobility sizes are generally used in the studies on size-resolved BC particles. For instant, Zhang et al. (2016) measured the morphology and density of internally mixed BC (In-BC for short in the reference) with SP2 and VTDMA. They used the peak diameter of the normalized volume size distribution of the In-BC core to represent the typical diameter of In-BC core at the prescribed mobility diameters selected by the DMA.

We originally considered the sharp increases in the number of particles with very small rBC mass resulted from the detection noises of SP2 for the smaller BC particles. As claimed by the manufacture, the lower BC detection limit is  $\sim 0.3 \text{ fg}$  per particle. Thus, data filter was performed by eliminating the particles with incandescence signal peak values lower than 100. This criterion is determined from the calibration curve by using Aquadag particles (Fig. S3 in the revised supplemental file). However, the distribution concentrated at the smaller masses still existed after the data filter. Initially, we suspected the smaller masses belonged to the thickly-coated BC particles which were not separated from the extBC particles using the time delay method. However, we found that the smaller masses also existed for the bare BC particles (i.e., Aquadag). As shown in Fig. R1 and Table R1, the particles with these smaller masses accounted for only 1~9% of the total particles (after data filter by eliminating the signal with incandescence peak value lower than 100) in the range of 140–200 nm in mobility diameter. This proportion gradually increased to  $\sim 37\%$  at 700 nm. Thus, these smaller masses should not be resulted only from the ‘remnant’ BC particles with thick coating. We still attribute these smaller masses to measurement noises.

The Gaussian fitting for the major peak can distinctly distinguish the singly charged particles from those with double or more charges for Aquadag particles (considered as bare BC particles). However, in the case of measurement for ambient particles, it is

more complex. First, the time delay approach used in this study can only distinguish the thickly-coated BC particles from those with thinly or without coating. A fraction of thinly- and/or even moderately-coated BC particles cannot be absolutely separated from the bare BC particles. Thus, a fraction of extBC particles claimed in this study might be thinly-coated ones. We considered the right tail of the distribution was also associated with these thinly-coated BC particles. These thinly-coated BC particles have a relatively more compact structure than the bare BC particles, resulting in larger masses in a given mobility diameter.

19. L252: Please provide further details for how the fit was performed. Were both the prefactor  $k$  and mass-mobility exponent  $D_f$  allowed to vary freely? The  $k$  value seems to be very low in comparison to previous measurements (Sorensen 2011 and references therein), which requires explanation. How is the standard deviation of 0.04 in  $D_f$  determined? How sensitive is the fitted  $D_f$  to the size-dependent measurement uncertainties in rBC mass?

**Reply:** Actually, a linear regression of  $\log(\text{mass})$  (e.g.,  $y$ ) against  $\log(d_{\text{mob}})$  (e.g.,  $x$ ) by minimizing the chi-square error statistic between the fitted  $\log(\text{mass})$  (e.g.,  $y_{\text{fit}}$ ) and measured ones. The chi-square error is calculated as  $\sum(y-y_{\text{fit}})^2$ . According to the mass-mobility exponential equation shown in Section 3.3 of the revision, the y-intercept of the linear regression should be  $\log(k)$ , and the slope is  $D_{\text{fm}}$ . We have corrected the definition of fractal dimension ( $D_f$ ) in our initial study and called  $D_{\text{fm}}$  as the mass-mobility scaling exponent. We also illustrate the difference in  $D_f$  and  $D_{\text{fm}}$  in the introduction section of the revision (Lines 100–106) according to the review literature (Sorensen, 2011). Thus, the prefactor  $k$  derived from the mass-mobility relationship cannot compare to that presented in Sorensen (2011). It seems to be comparable to the value presented in previous DMA-APM measurements for the soot aggregates. For instance, the prefactor value is  $\sim 6\text{--}8 \times 10^{-6}$  (Park et al., 2003), close to the value presented in our study. The prefactor of mass-mobility relationship is with few concern in previous studies.

The standard deviation in  $D_{\text{fm}}$  is derived as the 1-sigma uncertainty estimates for the slope of linear regression of extBC mass against  $d_{\text{mob}}$  at the logarithmic scale. The uncertainty in the determination of extBC was estimated to be  $\sim 20\%$  at each  $d_{\text{mob}}$ , including the uncertainty in the rBC mass determined by the SP2 and that raised from the time delay method used to discriminate extBC. Similar discussion can be found in our revised manuscript, e.g., Lines 358–365, 463–469.

20. Fig. 3: Error bars are required in this figure to indicate the measurement

uncertainties.

**Reply:** The typically mass of extBC was determined from the lognormal fitting. We also show the uncertainties in the revised Fig. 3 and Fig. 4, and discuss the uncertainties explicitly in the main content (e.g., Lines 481–499).

21. L263: This is a speculative statement that is not examined as thoroughly as it should be. If the sensitivity of  $D_f$  to measurement uncertainty is taken into consideration is it still possible to conclude that the  $D_f$  calculated here is 'relatively lower' than the previous measurements? If this result stands, can the authors provide any evidence to support their claim that fuel quality is higher in Beijing than for the studies they have cited?

**Reply:** The extBC mass determined at a given  $d_{\text{mob}}$  is expected to have ~20% uncertainty as presented in the revision. The uncertainties should be similar at different mobility size. Thus, the  $D_{\text{fm}}$ , calculated as the scaling exponent of the mass-mobility relationship should be influenced relatively low by the uncertainty in extBC mass. I mean the synchronous variations in extBC masses due to uncertainty at different  $d_{\text{mob}}$  should have few effects on the  $D_{\text{fm}}$ . In the revision, we also examine the sensitivity of  $D_{\text{fm}}$  to the  $d_{\text{mob}}$  range in which the power law function is used to fit the mass-mobility relationship. The  $D_{\text{fm}}$  fitted in 140–350 nm  $d_{\text{mob}}$  range (2.51) is significantly larger than that fitted in 350–750 nm (2.07). It indicates the smaller extBC particles are more likely influenced by the reconstruction effect than the larger extBC (Lines 433–440).

The fuel quality is very strict in Beijing. The JING VI standard was implemented from year of 2017. We have no explicit information of the fuel quality. However, at least, we know the sulfate content is very low in the fuel with JING VI standard, which will have an important impact on the structure of BC aggregates. Besides, the local government claimed that the nitrogen oxides, particulate matters, total hydrocarbons and carbon monoxides emitted from the diesel exhausts are expected to decrease by factors of 4.6%, 9.1%, 8.3% and 2.2% respectively if the fuel with JING VI standard is used.

22. L337: 'extBC' as defined with respect to delay time could also be comprised of BC mixed with small or even moderate amounts of non-BC material (e.g. L280). Additionally, the measurements reported here are lower than previous DMA-SP2 measurements of effective density in Beijing. Therefore, I find this explanation of the low effective density values measured in this study to be problematic.

**Reply:** We have removed the discussion in diurnal variation in  $D_{\text{fm}}$  due to the enlarged uncertainty of insufficient data volume in the revision. Instead, we discuss the differences in the mass-mobility relationship between a polluted episode and a clean

period. Although a fraction of the thinly- and/or even moderately-coated BC might be recognized as extBC using the time delay discrimination, these particles should have few effects on the determined typical extBC mass at each  $d_{\text{mob}}$ . Explicit discussions have been presented in our revised manuscript (Lines 331–365). Increase in the volatile and/or semi-volatile materials accompanied with the BC aggregates would increase the possibility of the BC aggregates becoming relatively more compact due to reconstruction effect. It will increase the mass, consequentially the effective density of extBC aggregates at a given  $d_{\text{mob}}$ . Even the structure of a BC aggregate changes little, small amounts of the volatile and/or semi-volatile materials filled in the gap and/or thinly-coated outside the primary spherules of BC aggregate would have few effects on its mobility but result in a higher mass of the entire particle. The increased mass can be detected by the APM but cannot be characterized by the SP2. Similar explanation is also presented in Lines 515–518 in the revision.

The effective density of internally mixed BC (In-BC, or thickly-coated BC) was measured by the previous DMA-SP2 system (Zhang et al., 2016). These In-BC particles have been reconstructed due to the thick coating. Thus, a compact structure with much higher density was reported. The fractal-like extBC aggregates without thick coating are studied in current study, which have low effective density.

## References

- Gao, R. S., Schwarz, J. P., Kelly, K. K., Fahey, D. W., Watts, L. A., Thompson, T. L., Spackman, J. R., Slowik, J. G., Cross, E. S., Han, J.-H., Davidovits, P., Onasch, T. B., and Worsnop, D. R.: A novel method for estimating light-scattering properties of soot aerosols using a modified single-particle soot photometer, *Aerosol Sci. Technol.*, 41, 125–135, doi:10.1080/02786820601118398, 2007.
- Gysel, M., Laborde, M., Olfert, J. S., Subramanian, R., and Gröhn, A. J.: Effective density of Aquadag and fullerene soot black carbon reference materials used for SP2 calibration, *Atmos. Meas. Tech.*, 4, 2851–2858, doi:10.5194/amt-4-2851-2011, 2011.
- Laborde, M., Mertes, P., Zieger, P., Dommen, J., Baltensperger, U., and Gysel, M.: Sensitivity of the Single Particle Soot Photometer to different black carbon types, *Atmos. Meas. Tech.*, 5, 1031–1043, doi:10.5194/amt-5-1031-2012, 2012.
- Park, K., Cao, F., Kittelson, D. B., and McMurry, P. H.: Relationship between particle mass and mobility for diesel exhaust particles, *Environ. Sci. Technol.*, 37, 577–583, doi:10.1021/es025960v, 2003.
- Raatikainen, T., Brus, D., Hooda, R. K., Hyvärinen, A.-P., Asmi, E., Sharma, V. P., Arola, A., and Lihavainen, H.: Size-selected black carbon mass distributions and mixing state in polluted and clean environments of northern India, *Atmos. Chem. Phys.*, 17, 371–383, doi:10.5194/acp-17-371-2017, 2017.
- Sorensen, C. M.: The mobility of fractal aggregates: A review, *Aerosol Sci. Technol.*, 45, 765–779, doi:10.1080/02786826.2011.560909, 2011.

- Taylor, J. W., Allan, J. D., Liu, D., Flynn, M., Weber, R., Zhang, X., Lefer, B. L., Grossberg, N., Flynn, J., and Coe, H.: Assessment of the sensitivity of core/shell parameters derived using the single particle soot photometer to density and refractive index, *Atmos. Meas. Tech.*, 8, 1701–1718, doi:10.5194/amt-8-1701-2015, 2015.
- Zhang, Y. X., Zhang, Q., Cheng, Y. F., Su, H., Kecorius, S., Wang, Z. B., Wu, Z. J., Hu, M., Zhu, T., Wiedensohler, A., and He, K. B.: Measuring the morphology and density of internally mixed black carbon with SP2 and VTDMA: new insight into the absorption enhancement of black carbon in the atmosphere, *Atmos. Meas. Tech.*, 9, 1833–1843, doi:10.5194/amt-9-1833-2016, 2016.

## Marked-up manuscript verison

# **A ~~novel~~ study of the morphology and effective density of externally mixed black carbon aerosols in ambient air using a size-resolved single-particle soot photometer (SP2)**

Yunfei Wu<sup>1\*</sup>, Yunjie Xia<sup>1, 2</sup>, Rujin Huang<sup>3</sup>, Zhaoze Deng<sup>4</sup>, Ping Tian<sup>5</sup>, Xiangao Xia<sup>4</sup>,  
Renjian Zhang<sup>1\*</sup>

1 Key Laboratory of Regional Climate-Environment for Temperate East Asia (RCE-TEA), Institute of Atmospheric Physics, Chinese Academy of Sciences, Beijing 100029, China

2 University of Chinese Academy of Sciences, Beijing, 100049, China

3 Key Laboratory of Aerosol Chemistry and Physics, State Key Laboratory of Loess and Quaternary Geology, Institute of Earth and Environment, Chinese Academy of Sciences, Xi'an 710061, China

4 Key Laboratory of Middle Atmosphere and Global Environment Observation (LAGEO), Institute of Atmospheric Physics, Chinese Academy of Sciences, Beijing 100029, China

5 Beijing Weather Modification Office, Beijing 100089, China

*Correspondence to:* Yunfei Wu (wuyf@mail.iap.ac.cn) and Renjian Zhang (zrj@mail.iap.ac.cn)

## **Abstract**

The morphology and effective density of externally mixed black carbon (*extBC*) aerosols, ~~an~~ important factors affecting the radiative forcing of black carbon, ~~was-were~~ studied by using a tandem ~~method-technique~~ coupling a differential mobility ~~diameter analyzer~~ (DMA) with a single-particle soot photometer (SP2). The study extended the mass-mobility relationship to large *extBC* particles with a mobility diameter ( $d_{mob}$ ) larger than 350 nm, a size range was seldom included in previous tandem measurements of BC aggregates in the atmosphere. The experiment was conduct at an urban site in Beijing during a 19-day winter period from 23 January to 10 February 2018. Ambient dry particles were selected by the DMA, and the size-resolved *extBC* particles were distinguished from ~~those-particles of-with~~ a thick coating (internally mixed) according

28 to the time delay between the incandescence signal peak and the scattering peak  
29 detected by the SP2 and .The masses of the extBC particles were then quantified by the  
30 SP2. The time differences between the DMA size selection and the SP2 measurement  
31 were processed previously, ~~as well as the effects of multicharged particles.~~ The  
32 normalized number size distributions were investigated at the prescribed  $d_{mob}$  sizes in  
33 the range of 140–750 nm to provide the typical mass of extBC at each  $d_{mob}$ . Based on  
34 this basis, the mass-mobility relationship of the ambient extBC was established,  
35 inferring the a fractal dimension of the extBC particles was obtained mass-mobility  
36 scaling exponent ( $D_{fm}$ ), (an important quantity for characterizing the morphology of  
37 fractal-like BC aggregates) with a value of  $2.3634 \pm 0.0403$  in the mobility range  
38 investigated in this study. This value is comparable with those of diesel exhaust  
39 particles, implying a predominant contribution of vehicle emissions to the ambient  
40 extBC in urban Beijing. Compared to the clean period, a higher  $D_{fm}$  value was observed  
41 in the polluted episode, indicating a more compact BC aggregate structure than that in  
42 the clean period. The effective densities ( $\rho_{eff}$ ) of the extBC in the same  $d_{mob}$  mobility  
43 diameter range of 140–750 nm were also derived, with values gradually decreasing  
44 from  $0.34\text{--}46$  g cm<sup>-3</sup> at 140–160 nm mobility to  $0.12\text{--}14$  g cm<sup>-3</sup> at 700–750 nm mobility.  
45 The  $\rho_{eff}$  values were generally slightly lower than those measured using the DMA-  
46 aerosol particle mass analyzer (APM) system. ~~This~~ The difference in  $\rho_{eff}$  values was  
47 most likely due to the lower BC masses determined by the SP2 compared to those ~~from~~  
48 measured by the APM at the same mobility, since the SP2 measured ~~the mass of pure~~  
49 the refractory BC (rBC) mass instead of the ~~entire total mass of the BC aggregate,~~  
50 which consisting consists of both ~~refractory rBC~~ and a possible fraction of  
51 nonrefractory components measured by the APM. Higher  $\rho_{eff}$  values were observed in  
52 the 280–350 nm  $d_{mob}$  range, and were much closer to the values for soot aggregates  
53 reported in the literature. The higher  $\rho_{eff}$  values might be related to the more compact  
54 structure of BC aggregates in this range, resulting from the reconstruction effect by  
55 volatile and/or semivolatile components in the atmosphere. The reconstruction effect  
56 might also result in a hiatus in the increased dynamic shape factor in the range of 200–  
57 350 nm which generally increased from 2.16 to 2.93 in the 140–750 nm  $d_{mob}$  range.

58

## 59 **1 Introduction**

60 Black carbon (BC), a byproduct of incomplete combustion, is the main light-absorbing  
61 component in atmospheric aerosols. BC can lead to positive radiative forcing only  
62 second to CO<sub>2</sub> and thus ~~Earth-warming~~ of the earth's atmosphere (IPCC, 2013).  
63 However, there remains a large amount of uncertainty regarding the radiative forcing  
64 induced by BC due to its complexity and variability in ~~the~~ morphology, mixing state  
65 and hygroscopicity. Freshly emitted BC particles usually exhibit as fractal-like  
66 ~~aggregates made chain-like agglomerates built up by of~~ a number of primary carbon  
67 spherules (Park et al., 2004; Sorensen, 2011), which are generally hydrophobic. The  
68 ~~C~~condensation of organic and/or inorganic components leads to ~~a the~~ collapse of the  
69 ~~chain like fractal-like aggregates agglomerates,~~ and, in turn, a compact structure of BC  
70 particles (Slowik et al., 2007; Zhang et al., 2008). Changes in the morphology of BC  
71 particles affect their optical properties. ~~Meanwhile, e~~Encasement by organic and/or  
72 inorganic coatings also increases the absorption of BC particles through the lensing  
73 effect (Shiraiwa et al., 2010; Peng et al., 2016). In addition, water-soluble coatings  
74 increase the hydrophilic ability of the BC particles (Zhang et al., 2008; McMeeking et  
75 al., 2011), indirectly affecting the radiative forcing by affecting the cloud processes.  
76 Laboratory studies indicate that freshly emitted BC particles can be thickly coated  
77 within a few hours in the atmosphere (Pagels et al., 2009; Peng et al., 2016). Thus,  
78 many studies have focused on the optical properties and radiative forcing of thickly-  
79 coated BC particles (Jacobson, 2001; Khalizov et al., 2009; Liu et al., 2017). However,  
80 *in situ* measurements have shown that a great number of uncoated and/or thinly-coated  
81 BC particles exist in the ambient atmosphere, with a fraction even higher than that of  
82 the aged BC particles (Schwarz et al., 2008). In general, thickly-coated BC particles  
83 account for <50% of the BC-containing particles in urban areas based on single-particle  
84 soot photometer (SP2) measurements (Huang et al., 2012; Wang et al., 2014; Wu et al.,  
85 2016). The existence of a large fraction of uncoated and/or thinly-coated BC particles  
86 is likely due to continuous emission from combustion processes such as vehicle exhaust  
87 (Wang et al., 2017). Therefore, studies on the radiative forcing of BC particles without

88 thick coatings are also essential, especially in urban areas. First, the morphologies and  
89 sizes of these quasi-bare BC particles ~~should be investigated, as they greatly impact~~  
90 ~~the~~ which are the essential quantities for calculating the optical properties of ~~the~~ BC  
91 particles in numerical models, should be investigated (Scarnato et al., 2013; Bi et al.,  
92 2013).

93 The morphology of fractal-like BC aggregates is generally characterized by a quantity  
94 called ‘fractal dimension’ ( $D_f$ ), which has been well documented in the review literature  
95 (Sorensen, 2011). The ideal diffusion-limited cluster aggregation (DLCA), to which the  
96 BC aggregates belong, has a  $D_f$  value of  $1.78 \pm 0.1$ . Recent studies have also reported  
97 a similar  $D_f$  value of  $\sim 1.82$  for bare-like soot particles by using transmission electron  
98 microscopy (TEM) analysis of aerosol samples collected in four different environments  
99 (Wang et al., 2017). A significant increase in the  $D_f$  was observed when the soot  
100 particles were partly coated or embedded. In the past two decades, the morphologies of  
101 the BC aggregates were also widely studied by using tandem mobility techniques (Park  
102 et al., 2008). Measurements obtained by using an impactor (e.g., the electrical low-  
103 pressure impactor (ELPI)) or a particle mass analyzer (e.g., the aerosol particle mass  
104 analyzer (APM), the centrifugal particle mass analyzer (CPMA)) connected in tandem  
105 with a differential mobility analyzer (DMA) revealed the relationship between particle  
106 mass and mobility (Park et al., 2003; Maricq and Xu, 2004; Olfert et al., 2007; Rissler  
107 et al., 2014; Sorensen, 2011; and associated references therein). The derived mass-  
108 mobility scaling exponents ( $D_{fm}$ ) which were also called ‘fractal dimensions’ in some  
109 of these references varied in a wide range of 2.2–2.8 for diesel exhaust particles. These  
110 values were inherently higher than the virtual  $D_f$  due to the improper interpretation of  
111 mobility measurements, which was demonstrated in detail in Sorensen (2011). The  $D_f$   
112 of diesel particles obtained using TEM is  $\sim 1.75$ , corresponding to a large  $D_{fm}$  value of  
113  $\sim 2.35$  obtained from the mass-mobility relationship (Park et al., 2004). The mobility  
114 size-dependent effective densities ( $\rho_{eff}$ ) of BC aggregates were also determined from  
115 the DMA-ELPI or DMA-APM (or CPMA) measurements which were difficult to  
116 characterize using the TEM techniques.

117 The previous tandem measurements generally provided the mass-mobility relationship

118 of particles with a mobility diameter ( $d_{mob}$ ) not exceeding 350 nm due to the system  
119 detect limit (Park et al., 2003; Maricq and Xu, 2004; Olfert et al., 2007; Rissler et al.,  
120 2014). A condensation particle counter (CPC) is connected next to the DMA-APM  
121 system to measure the number concentrations of mobility size-selected particles at  
122 various APM voltages. The voltage is proportional to the particle mass, and the voltage  
123 resulting in the maximum concentration is considered the typical voltage, in turn, of the  
124 mass of particles with a prescribed mobility size. Because the larger particles (e.g.,  
125  $d_{mob}>350$  nm) are less abundant in the atmosphere than the smaller particles, larger  
126 uncertainties exist in the DMA-APM-CPC measurements for these larger particles  
127 (Geller et al., 2006). The applicability of the mass-mobility relationship established on  
128 the basis of tandem measurements of smaller mobility diameters (e.g.,  $d_{mob}<350$  nm) to  
129 larger particles (e.g.,  $d_{mob}>350$  nm) is insufficient. The morphology of agglomerate BC  
130 particles is often studied directly using transmission electron microscopy (TEM) (Park  
131 et al., 2004). However, the timeliness and representation of filter-based TEM  
132 measurements is challenged because only a small fraction of particles on the filter  
133 collected during a considerable period are investigated (Wentzel et al. 2003). By  
134 comparison, online tandem techniques can provide much more efficient and  
135 representative measurements of particle properties, including morphology (Park et al.,  
136 2008). For example, based on the measurements of an electrical low pressure impactor  
137 (ELPI) or an aerosol particle mass analyzer (APM) in tandem with a differential  
138 mobility analyzer (DMA), the fractal dimension, a crucial representative aspect of the  
139 morphology of agglomerate BC particles, has been studied (Park et al., 2003; Maricq  
140 and Xu, 2004; Olfert et al., 2007; Rissler et al., 2014). The effective density and the  
141 dynamic shape factor of these agglomerates can also be obtained from tandem  
142 measurements. Generally, a condensation particle counter (CPC) connected to an APM  
143 is used to obtain the typical mass of the size selected particles from the DMA, which is  
144 determined as the mass corresponding to the peak APM voltage that results in the  
145 maximum particle number concentration. There exist large uncertainties from CPC  
146 detection when the particle concentration is low. Thus, the DMA-APM measurement is  
147 usually limited to relatively small particles that are abundant in the atmosphere (Geller

148 ~~et al., 2006). The upper size limit of the measured particles using the DMA APM~~  
149 ~~system is generally not larger than 400 nm in mobility diameter (Park et al., 2003;~~  
150 ~~Maricq and Xu, 2004; Olfert et al., 2007; Rissler et al., 2014).~~

151 The SP2 was developed on the basis of the laser-induced incandescence technique ~~was~~  
152 ~~widely used to study BC aerosol properties~~ and provides an advantage to the study of  
153 individual BC particle properties, including mass, size and mixing state. ~~†The SP2~~  
154 determines the refractory BC (rBC) mass from particle to particle ~~with, thus providing~~  
155 the masses of BC aggregates throughout a wide size range (70–500 nm mass-equivalent  
156 diameter claimed by the manufacturer) with very high precision sensitivity and  
157 accuracy and distinguishes the BC aggregates with or without thin coatings from the  
158 thickly coated BC particles (Schwarz et al., 2006; ~~Moteki and Kondo, 2007~~). Recently,  
159 a tandem system consisting of an SP2 connected next to a DMA was developed to study  
160 the properties of size-resolved BC aerosols in the atmosphere. The mass distributions  
161 and mixing states of the size-selected BC were investigated in northern India by using  
162 a DMA-SP2 tandem system (Raatikainen et al., 2017). Coupling an SP2 with a  
163 volatility tandem DMA (VTDMA), rBC core size distributions of internally mixed BC  
164 and those measured by the VTDMA were compared at the prescribed mobility size  
165 ranges. Subsequently, the morphology and effective density of the internally mixed BC  
166 particles were studied (Zhang et al., 2016). The hygroscopic properties of BC particles  
167 were studied by using a hygroscopicity tandem DMA (HTDMA)-SP2 coupling system  
168 (McMeeking et al., 2011; Liu et al., 2013). Few studies have been performed on the  
169 morphology and effective density of fractal-like BC aggregates uncoated by other  
170 components using the DMA-SP2 measurement, especially in the ambient atmosphere.  
171 Using the DMA-SP2/CPC system, Gysel et al. (2012) revealed that the SP2 was unable  
172 to reliably detect BC particles from a PALAS spark discharge soot generator due to the  
173 lower detection limit of the SP2 for loosely packed agglomerates made up of small  
174 primary spherules (~5–10 nm in diameter). However, they also claimed that a well-  
175 aligned SP2 was expected to have a detection efficiency adequate to measure the BC  
176 aggregates (e.g., diesel exhaust soot) in the atmosphere because these BC aggregates  
177 have larger primary spherules and substantially higher effective densities than the

178 agglomerates made up of small primary spherules. Therefore, in this study, a DMA-  
179 SP2 tandem system was built to examine the mass-mobility relationship (from which  
180 the morphology and effective density were further derived) of uncoated BC aggregates,  
181 especially in the large particle size range (e.g.,  $d_{\text{mob}} > 350$  nm) which was seldom  
182 included in previous tandem measurements. Moreover, the uncoated BC aggregates  
183 were distinguished from the thickly-coated BC particles by using the SP2, allowing the  
184 study on the mass-mobility relationship of ambient BC aggregates in different  
185 atmospheric environments. Previous DMA-ELPI or APM tandem measurements were  
186 mainly conducted in the laboratory or in the source environments (e.g., in the tunnel)  
187 where fresh BC aggregates were predominant.

188 Beijing, the capital of China, has suffered from severe air pollution issues in recent  
189 years. Studies have revealed that emissions from coal combustion and/or biomass  
190 burning for industry activities and residential heating have played a predominate role  
191 in the particulate pollution in Beijing, especially in the polluted episodes (Zhang et al.,  
192 2013; Huang et al., 2014; Wu et al., 2017; Ma et al., 2017a,b). Thus, the variation in the  
193 mass-mobility relationship of uncoated BC aggregates was also compared for a polluted  
194 episode and a clean episode to examine the possible influence of source change on the  
195 morphology of these BC aggregates. In addition, a better mobility size resolution (33  
196 logarithmic size bins from 20 to 750 nm) was set for our DMA-SP2 system than that  
197 used in previous similar studies in which only a few mobility diameters in the range of  
198 ~150–350 nm were selected (Zhang et al., 2016; Liu et al., 2013; McMeeking et al.,  
199 2011). Similar to the study presented in Raatikainen et al. (2017), the high size  
200 resolution provides an advantage for calculating the BC mass and number size  
201 distribution in the polluted region in our future studies.

202 ~~In this study, we developed a system consisting of an SP2 connected in tandem with the~~  
203 ~~DMA. This system was used to study the morphology of the BC aggregates from ~100~~  
204 ~~nm to 750 nm in mobility diameter. An advantage of this system is that the SP2~~  
205 ~~measures the mass of pure BC instead of the entire mass of the BC containing particles~~  
206 ~~that was determined using the APM or ELPI in previous studies, leading to a more~~  
207 ~~accurate detection of the effective density of the BC aggregates. Meanwhile, the size~~

208 ~~limitation for BC aggregate detection is expanded to 750 nm in mobility diameter,~~  
209 ~~providing more comprehensive knowledge on the morphology of the BC aggregates in~~  
210 ~~ambient air. Using this novel tandem system, the fractal dimension, effective density~~  
211 ~~and dynamic shape factor of ambient BC aggregates were investigated, providing~~  
212 ~~important insights for better assessment of the regional radiative effects of agglomerate~~  
213 ~~BC particles.~~

## 214

## 215 **2 Methodology**Measurements

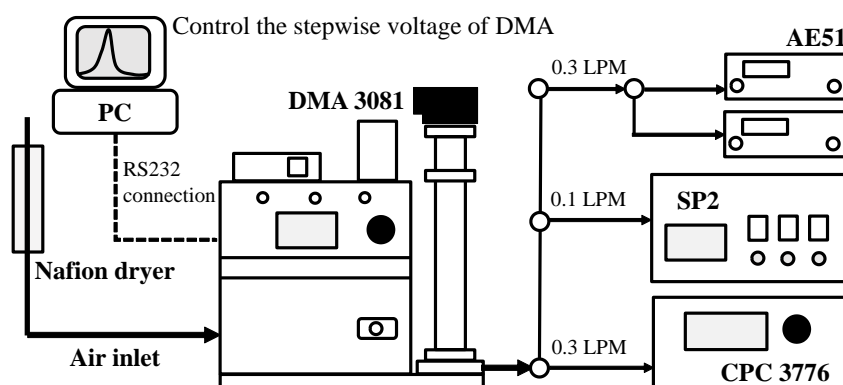
### 216 **2.1 Experimental setup**

217 ~~The A tandem system comprises a size selection unit and a measurement section was~~  
218 ~~built, and deployed in an ambient experiment that was conducted on the roof of a~~  
219 ~~building (approximately 8 m above the ground) on the campus of the Institute of~~  
220 ~~Atmospheric Physics, Chinese Academy of Sciences (IAP, CAS) during the winter~~  
221 ~~from 23 January to 10 February 2018 (19 days in total). The site is located in an urban~~  
222 ~~area of Beijing; it is a few hundred meters away from two main roads and thus may be~~  
223 ~~significantly affected by vehicle emissions. More information about the measurement~~  
224 ~~site is described in previous studies (e.g., Wu et al., 2016, 2017).~~

225 As shown in Fig. 1, ~~a sample of air polydisperse aerosols in the sample air was were~~  
226 ~~drawn through the size selection unit (a model 3087 neutralizer-DMA, a model 3080~~  
227 ~~classifier and a model 3081 DMA, TSI Inc., Shoreview, MN, USA) to generate quasi-~~  
228 ~~monodisperse particles with a certain electrical  $d_{\text{mob}}$  mobility diameter. Before entering~~  
229 ~~the system, the ambient air was dried prior to passing through a 12-inch-long Nafion~~  
230 ~~dryer (model MD-700-12F-3, Perma Pure LLC, Toms River, NJ, USA). A vacuum~~  
231 ~~pump was used to draw the dry sheath air (e.g., particle-free indoor air) opposite to the~~  
232 ~~flow direction of the sample air to provide an appropriate vacuum degree required for~~  
233 ~~the dryer.~~ The size-selected particles were delivered to the measurement section for  
234 analysis by various methods, including an SP2 (Droplet Measurement Technologies,  
235 Boulder, CO, USA), a CPC (model 3776, TSI Inc., Shoreview, MN, USA) and two  
236 microaethalometers (model AE51, ~~Aethlab~~AethLabs, San Francisco, CA, USA). The  
237 operational flow rates were set to 0.1, 0.3 and 0.15 LPM (STP) for the SP2, CPC and

238 ~~two AE51s~~, respectively. The sheath flow ~~ratio-rate~~ was set to 3 LPM, resulting in a  
 239 ratio of ~~sheath-sheath-to-to~~-sample flow rate of 4.3:1 for the DMA. Particles in the range  
 240 of 15–750 nm in mobility diameter ~~can-could~~ be selected. The flow rate for each  
 241 instrument was calibrated using a soap film flowmeter (model Gilian Gilibrator-2,  
 242 Sensidyne, Petersburg, FL, USA) before the experiment to ensure the accuracy of the  
 243 selected particle sizes and measurements. ~~The scientific purpose of this experimental~~  
 244 ~~setup was to study the mixing states of size-selected BC particles, the mass and number~~  
 245 ~~size distribution of BC, as well as the morphology and effective density of the uncoated~~  
 246 ~~BC aggregates that are discussed in the current study. Since only the DMA and SP2~~  
 247 ~~were involved in the measurements presented in this study, the setting and operation of~~  
 248 ~~the two instruments~~~~This study mainly were describes-described~~ and ~~diseusses-discussed~~  
 249 ~~in detail~~~~the DMA-SP2 measurement.~~

250



251

252 Fig. 1 Schematic of the experimental setup for size-resolved measurements of black  
 253 carbon.

254

## 255 2.2 Particle size selection

256 ~~An ambient experiment was conducted on the roof of a building (approximately 8 m~~  
 257 ~~above the ground) on the campus of the Institute of Atmospheric Physics, Chinese~~  
 258 ~~Academy of Sciences (IAP, CAS) during the winter period from 23 January to 10~~  
 259 ~~February 2018 (19 days in total). The site is located in an urban area of Beijing. It is a~~  
 260 ~~few hundred meters away from two main roads and thus may be significantly affected~~  
 261 ~~by vehicle emissions. More information about the measurement site is described in~~

262 ~~previous studies (e.g., Wu et al., 2016, 2017). The ambient air was dried by passing~~  
263 ~~through a nafion dryer (model MD-700, Perma Pure LLC) before entering the system.~~  
264 The DMA was connected to an external computer on which a program was run to  
265 control the voltage of the DMA, i.e., the particle mobility diameter ( $d_{mob}$ ). Thirty-three  
266 mobility diameters were set in the program to cyclically control the particles selected  
267 by the DMA ~~and gradually increasing~~ increased from 20 nm to 750 nm at the  
268 logarithmic scale. Stepwise size selection was repeated until the operator stopped the  
269 program. A short cycle with each of the 33 diameters lasting for 18 s and a long cycle  
270 with each size lasting for 36 s were set to alternately operate in this experiment (Fig.  
271 ~~S2S1~~ S2S1 in the supplemental file). The purpose of this setting was to identify the time  
272 difference between the size selection and the subsequent measurement, as described in  
273 the following sections.

### 274 275 **2.3 Black carbon measurement**

276 The individual particulate rBC mass was measured by the SP2 according to the laser-  
277 induced incandescence signal when the BCparticle passed through the intense Nd:YAG  
278 intracavity continuous laser beam (Schwardz et al., 2006) with a Gaussian distribution.  
279 The rBC mass in the SP2 detection range (~0.3–250 fg in this study, dependent on the  
280 laser intensity of a specific instrument) is proportional to the peak of the incandescence  
281 signal independent of the mixing state of the BC particles. If a BC particle is coated  
282 with nonrefractory components, the coating will evaporate before the rBC core  
283 incandesces, leading to a time lag between the peaks of incandescence and scattering  
284 signals that are synchronously detected by the SP2 (Moteki and Kondo, 2007).  
285 According to the frequency distribution of the time lag, there was a significant  
286 distinction between thickly-coated (i.e., internally mixed) BC particles (intBC) and  
287 thinly-coated or uncoated (i.e., externally mixed) ~~ones~~ BC particles (extBC) (Fig. ~~S4S2~~  
288 with a minimum frequency at ~2  $\mu$ s. BC-containing particles with a delay times lag  
289 shorter than 2  $\mu$ s were identified as extBC ~~externally mixed~~. The delay time ~~delay~~  
290 threshold might vary slightly from one SP2 to another, e.g., Zhang et al. (2016) reported  
291 a short time lag of 1.6  $\mu$ s. However, it the delay time threshold should be constant for a

292 given instrument. In previous measurements using the same SP2 employed in this study,  
293 the critical delay time ~~lag~~ was maintained at 2  $\mu\text{s}$  regardless of the ambient conditions,  
294 such as the pollution level (Wu et al., 2016, 2017). A fraction of BC-containing particles  
295 with thin or even moderate coatings might also be recognized as *ext*BC using the time-  
296 delay approach (Laborde et al., 2012). The effects of these thinly or even moderately  
297 coated BC particles will be discussed in Section 3.2 by reducing the delay time  
298 threshold from 2  $\mu\text{s}$  to 1.2  $\mu\text{s}$  and 0.4  $\mu\text{s}$ , respectively.

299 The scattering signal of a single particle synchronously detected by the SP2 can be used  
300 to estimate the optical size of the particle. The mixing state of a BC-containing particle  
301 can be deduced by comparing the optical size of the particle and the mass-equivalent  
302 size of the rBC core. Since the nonrefractory coating of a BC-containing particle is  
303 evaporated due to the light absorption and heating of the rBC core when it passes  
304 through the laser beam, the scattering cross-section of this particle, which is  
305 proportional to the scattering intensity at a given incident light intensity, is gradually  
306 decreased. To estimate the initial optical size of this particle, an approach called  
307 leading-edge-only (LEO) fitting was developed (Gao et al., 2007). A small fraction of  
308 the measured scattering signal at its initial stage before the particle is perturbed by the  
309 laser is employed in the LEO fitting to reconstruct the expected scattering distribution  
310 of the initial particle. In this method, the location of the leading edge in the beam is also  
311 required, which is determined from a two-element avalanche photodiode (APD) signal.  
312 Unfortunately, the notch in the two-element APD of our SP2 failed to fix in an adequate  
313 position (e.g., before the peak location of the laser beam) in this experiment. Thus, the  
314 optical size and the consequent coating thickness of the BC-containing particle cannot  
315 be estimated. However, the coating thickness is not a crucial quantity in our current  
316 study on the morphology and density of uncoated BC aggregates. The coating thickness  
317 can provide a validation of our discrimination of *ext*BC but should have little influence  
318 on our final analysis and the discussion presented in the following sections.

319 Before the experiment, the incandescence signal was calibrated using DMA-selected  
320 monodisperse Aquadag particles. The effective ~~density~~ densities of the mobility size-  
321 selected Aquadag particles ~~was~~ were referred to the polynomial equation as a function

of the  $d_{mob}$  reported by in Gysel et al. (2011). Since the incandescence signal is more sensitive to the Aquadag particles than to the ambient BC particles, i.e., the Aquadag particle induces a higher incandescence signal peak (by a factor of ~25%) than fullerene soot or an ambient BC particle with the same mass (Laborde et al., 2012). Thus, the peak intensity of the incandescence signal was reduced by a factor of 25% when calculating the calibration coefficient (Laborde et al., 2012). The same calibration was performed again after the experiment. The calibration factors varied little (<3%), to ensure indicating the stability of the SP2 measurement during the entire experiment (Fig. S3). The uncertainty in the individual rBC mass determination is estimated to be ~10% due to the uncertainties in the rBC mass calibration and the effective density of the calibration material. An additional uncertainty may also arise in the determination of extBC masses when the time-delay approach is used to distinguish the mixing state of BC particles. The uncertainty will be further discussed in Section 3.2.

#### ~~2.4 Theoretical calculation of the morphology and effective density~~

~~The structure of the externally mixed BC (extBC), agglomerated by primary spherules with diameters of 20-60 nm (Alexander et al., 2008), can be characterized by a mathematical parameter, the fractal dimension ( $D_f$ ), which is approximately expressed as a power law relationship between the mass of the agglomerate particle ( $m$ ) and its mobility diameter ( $d_{mob}$ ), expressed as~~

$$m = k \cdot d_{mob}^{D_f}$$

~~where  $k$  is a constant. It should be noted that the approximation is applied only when the  $D_f$  is greater than 2, the regime in which the extBC particles are generally located (Park et al., 2003). The  $D_f$  value of a sphere is 3. Thus, a particle is closer and closer to a sphere if the  $D_f$  increases gradually to 3.~~

~~The effective density ( $\rho_{eff}$ ) of the extBC particles is calculated as the ratio of the BC mass ( $m$ ) measured using the SP2 and its volume based on the mobility diameter selected by the DMA, expressed as~~

$$\rho_{eff} = \frac{6m}{\pi d_{mob}^3}$$

351 ~~Combining Eq. 1 and 2,  $\rho_{eff}$  can also be expressed as a function of  $d_{mob}$ ,~~

$$352 \quad \rho_{eff} = K \cdot d_{mob}^{D_f-3}$$

353 ~~The dynamic shape factor is also calculated to indicate the morphology of the extBC~~  
354 ~~particles. It is derived from the ratio of the slip-corrected mass equivalent diameter ( $d_{me}$ )~~  
355 ~~and  $d_{mob}$ , expressed as~~

$$356 \quad \chi = \frac{d_{mob} \cdot C_e(d_{me})}{d_{me} \cdot C_e(d_{mob})}$$

357 ~~where  $d_{me}$  is calculated from the BC mass ( $m$ ) by assuming the BC particle to be a~~  
358 ~~compact sphere with density  $1.8 \text{ g cm}^{-3}$ , and  $C_e$  is the Cunningham slip correction factor~~  
359 ~~parameterized by particle diameter ( $d$ )~~

$$360 \quad C_e(d) = 1 + \frac{2\lambda}{d} \left[ \alpha + \beta \exp\left(-\frac{\gamma \cdot d}{2\lambda}\right) \right]$$

361 ~~where  $\lambda$  is the mean free path of the gas molecules, which is set to 65 nm in this study~~  
362 ~~according to Zhang et al. (2016). The values of the three empirical parameters  $\alpha$ ,  $\beta$  and~~  
363  ~~$\gamma$  are 1.257, 0.4 and 1.1, respectively (Eq. 9.34 at Page 407 in Seinfeld and Pandis,~~  
364 ~~2006).~~

### 366 **3 Data ~~processes~~processing**

#### 367 **3.1 Identifying the time difference between the size selection and the SP2** 368 **measurement**

369 There exists a considerable difference between the time recorded by the size selection  
370 program and that recorded by the SP2, due to the time cost of the particles transmitting  
371 from the DMA to the SP2, as well as the system clock difference between the computer  
372 on which the size selection program runs and that for the SP2 data acquisition. As  
373 shown in Fig. ~~S2S1~~, the SP2 measurement ~~is occurs~~ significantly later than the size  
374 selection.

375 ~~There are~~ We develop two methods to identify the time difference. The first method is  
376 to find the time difference between the local peak in the particle number concentration  
377 (including both scattering and incandescence) detected by the SP2 and the beginning of  
378 the corresponding size selection cycle. During the experiment, stepwise size selection  
379 was cyclically ~~operated~~ performed to produce quasi-monodisperse particles with sizes

380 gradually increasing from 20 nm to 750 nm. Thus, at the beginning of each new cycle,  
381 the voltage of the DMA should first drop drastically from a high value to a low one to  
382 make the particle size decrease from 750 nm to 20 nm. As a result, some particles with  
383 sizes in the SP2 efficiently detectable range (~100–500 nm) ~~would be~~ measured  
384 during the descent period, producing a local peak in the number concentration. Since it  
385 takes only ~~several a few~~ seconds for the descent, identifying the occurrence time of the  
386 local peak position in the SP2 clock and the beginning time of the size selection in the  
387 external computer clock will provide the time difference of each cycle. ~~This method~~  
388 ~~was utilized in this study.~~

389 The other method is to check the consistency of the number and/or mass size  
390 distributions between the short-duration cycle and long-duration cycle. Although the  
391 durations of each size in the short cycle and long cycle are different (18 s vs. 36 s), the  
392 time difference between ~~the~~ size selection and the ~~SP2~~ measurement should be uniform  
393 for adjacent short and long cycles. Setting an initial time difference and calculating the  
394 mean number and/or mass concentration of each particle size, the number and/or mass  
395 size distributions are obtained. Then, the correlation coefficients between the size  
396 distributions during short and long cycles are calculated. Changing the time difference  
397 gradually, we can obtain a set of correlation coefficients as ~~a~~ functions of the time  
398 differences. The time difference resulting in ~~a~~ the maximum correlation coefficient ~~was~~  
399 ~~is~~ considered ~~as~~ the difference between the size selection and the ~~SP2~~ measurement.

400 ~~Since the detection efficiency of the SP2 decreases dramatically in the small particle~~  
401 ~~range (Fig. S4), the size distributions of the SP2-detected particles are inadequate for~~  
402 ~~further calculation of the correlation coefficients. Therefore, the former method was~~  
403 ~~employed in current study to identify the time difference between the size selection and~~  
404 ~~the SP2 measurement. The latter method will be used to examine the time difference~~  
405 ~~between the size selection and the AE51/CPC measurements in our future study on the~~  
406 ~~number and mass size distributions of BC.~~

407

408 ~~3.2 Minimizing the multicharged particles~~ Determination of the typical masses of  
409 extBC at prescribed mobility sizes

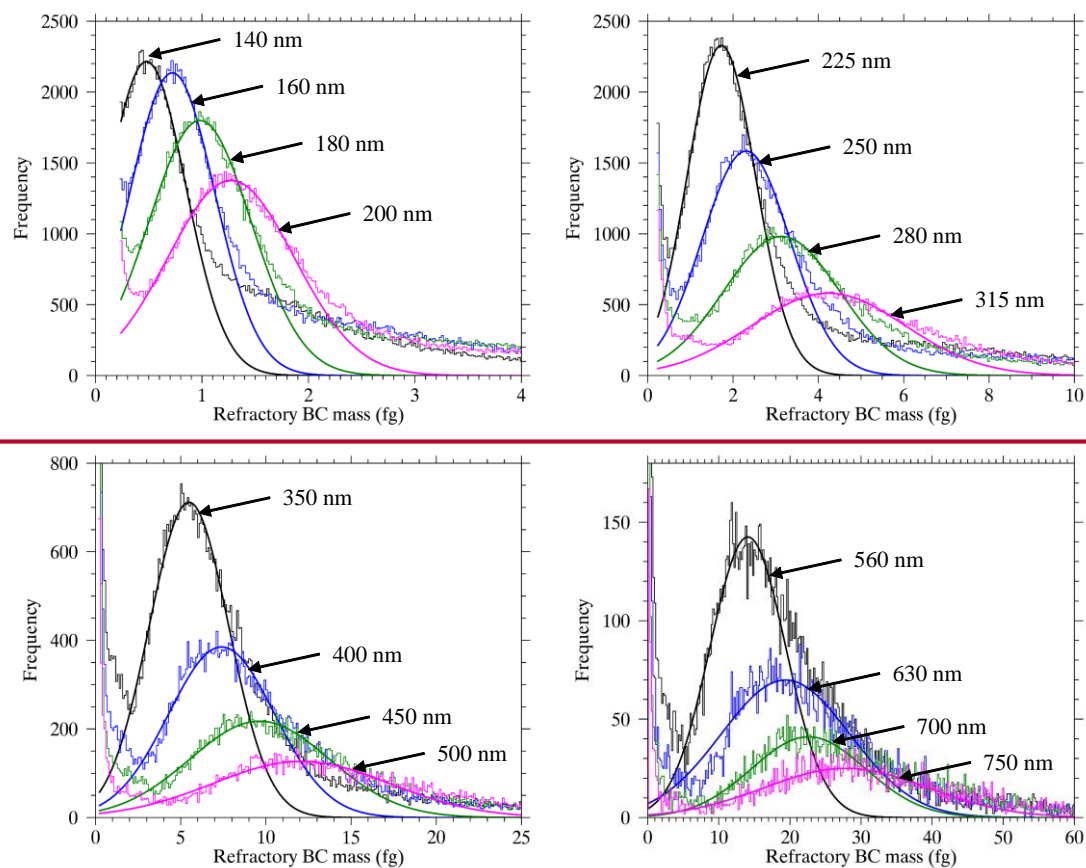
410 Particles in a certain size range are selected by the DMA instead of absolutely  
411 monodisperse particles at a given mobility size due to the effect of the transfer function.  
412 In addition, larger particles with multiple charges are also selected. The frequency and  
413 number size distributions of *extBC* as a function of the mass-equivalent diameter of  
414 rBC ( $d_{me}$ ) at different mobility sizes are presented in Fig. S5 and S6, respectively. Note  
415 that the number size distribution has been normalized by the peak value of the  
416 corresponding distribution. Since the frequency and number size distributions of *extBC*  
417 are quite insufficient at small particle sizes ( $d_{me} < 70$  nm) due to the low detection  
418 efficiency of the SP2 (Fig. S4), only the distributions with a  $d_{mob}$  larger than 140 nm  
419 are presented. In our following study, we mainly address the morphology and effective  
420 density of *extBC* in the 140–750 nm  $d_{mob}$  range. The normalized number size  
421 distributions at five representative  $d_{mob}$  (e.g., 140, 225, 350, 500, 750 nm) are also  
422 shown in Fig. 2. The *extBC* particles having a considerable  $d_{me}$  range were observed  
423 for a certain  $d_{mob}$ , indicating a wide transfer function of the DMA due to the relatively  
424 low ratio of sheath-to-sample flow (4.3:1). Multicharged particles also affected the size  
425 distribution, especially in the  $d_{mob}$  range of 100–400 nm (Ning et al., 2013). As shown  
426 in Fig. S6 and Fig. 2, a minor peak is obviously observed at the right tail of the major  
427 peak at each size distribution with a  $d_{mob} < 350$  nm.

428 As mentioned above, a fraction of thinly and/or moderately coated BC particles might  
429 also be recognized as *extBC* according to the time delay between the SP2 incandescence  
430 and scattering signal peaks. These particles also have impacts on the size distribution  
431 of *extBC* at a given mobility size. A thinly-coated BC particle can be expected to have  
432 a larger mass than a bare BC with the same mobility due to the restructuring of the  
433 thinly coated BC particle by coating materials. These thinly coated BC particles will  
434 increase the size distribution at their right tail when mixed with the effect of  
435 multicharged particles. It is difficult or even impossible to separate the effects of the  
436 thinly coated and multicharged particles based on the size distribution of *extBC* at the  
437 current stage. To examine the possible effect of these thinly coated particles, we  
438 tightened the criterion of the delay time for the discrimination of *extBC*, gradually  
439 decreasing from  $< 2.0$   $\mu$ s to  $< 1.2$   $\mu$ s and  $< 0.4$   $\mu$ s. As shown in Fig. S5 and S6, a decrease

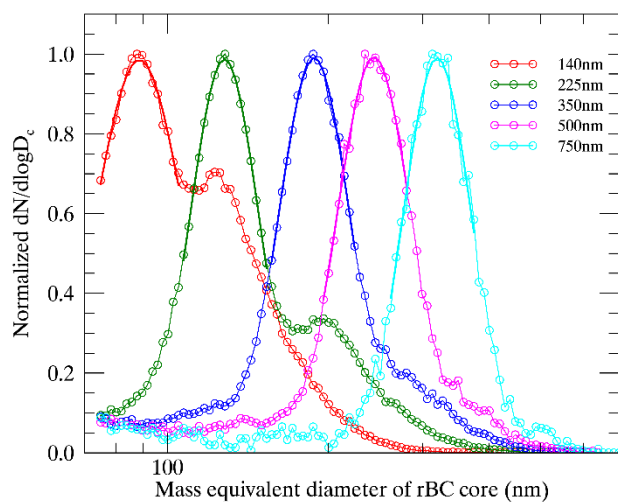
440 in the delay time threshold results in a significant reduction in the data volume used in  
441 the analysis but has few effects on the major peak location of the distribution, which is  
442 used as the typical  $d_{me}$  of *extBC* at a given mobility size. The typical  $d_{me}$  values,  
443 determined as the mode values of the lognormal function that are employed to fit the  
444 major peak of the size distribution at a certain mobility size, vary little with the delay  
445 time thresholds (Table S1). The maximum discrepancy in the  $d_{me}$  is <3% throughout  
446 the prescribed mobility size range in this study (140–750 nm). The delay time  
447 threshold-caused change mainly appears at the right tail of the normalized number size  
448 distribution. Reducing the delay time threshold to 0.4  $\mu$ s results in a significant decrease  
449 in the fraction of particles with a large  $d_{me}$  compared to the 2.0  $\mu$ s and 1.2  $\mu$ s thresholds  
450 (Fig. S6). These large particles are likely attributed to thinly and/or even moderately  
451 coated BC particles whose structures are relatively more compact than the absolutely  
452 bare BC particles. Therefore, we propose that thinly and/or even moderately coated BC  
453 and multicharged particles should both have effects on the size distribution of *extBC*,  
454 mainly at its right tail, while having little influence on the typical  $d_{me}$  that is considered  
455 as the peak  $d_{me}$  of the distribution at a given mobility size. The uncertainty in the typical  
456  $d_{me}$  due to the time-delay approach that was utilized to distinguish the *extBC* is  
457 approximately 3% at a given  $d_{mob}$ , which is in turn ~10% in the corresponding mass of  
458 *extBC*. Combining the uncertainty in the rBC mass determined by the SP2 (~10%), the  
459 total uncertainty in the determined mass of *extBC* should be ~20% in the studied  
460 mobility range of 140–700 nm. For the adequate data volume used in the analysis, the  
461 results and discussion presented in the following sections are based on the database of  
462 *extBC* discriminated as BC-containing particles with delay times lower than 2.0  $\mu$ s,  
463 unless otherwise specified.

464 ~~The typical mass of *extBC* at a given  $d_{mob}$  was affected by multicharged particles,~~  
465 ~~especially in the size range of 100–400 nm (Ning et al., 2013). If the simple average of~~  
466 ~~the individual *extBC* masses at a given  $d_{mob}$  was employed, the typical *extBC* mass~~  
467 ~~would be overestimated, resulting in measurement bias in the morphology of the *extBC*~~  
468 ~~particles, such as an overestimation in  $\rho_{eff}$  and an underestimation in  $\chi$ . Thus, following~~  
469 ~~the approach in the SP2 calibration process, Gaussian fitting was performed for the~~

470 frequency of *ext*BC mass at each  $d_{mob}$ . The major peak mass was considered as the mass  
 471 of singly charged *ext*BC particles corresponding to the given  $d_{mob}$  (Fig. 2). Due to the  
 472 detection limit of the SP2 for small BC particles with masses lower than  $\sim 0.3$  fg, only  
 473 the frequency of the *ext*BC mass with sizes larger than 125 nm in  $d_{mob}$  could be fit by a  
 474 Gaussian function. Thus, the typical *ext*BC masses at sixteen  $d_{mob}$  in the range of 140–  
 475 750 nm were obtained, as shown in Fig. 2 and Fig. 3.



476



477

478 Fig. 2 Campaign average number size distribution of the mass-equivalent diameter of  
 479 the rBC core of extBC normalized by the peak value at five represented mobility  
 480 diameters (140, 225, 350, 500 and 750 nm) selected by the DMA. Lognormal fitting is  
 481 performed for the major peak of each distribution. Frequency distribution of the mass  
 482 of the extBC particles selected at different mobility diameters. Gaussian fitting was  
 483 applied to the major peak of each distribution to deliver the representative extBC mass  
 484 for a certain mobility diameter.

### 486 2.4.3.3 Theoretical calculation of the morphology and effective density

487 The structure of the externally mixed BC (extBC), agglomerated by primary spherules  
 488 with diameters of 20-60 nm (Alexander et al., 2008), can be characterized by its mass-  
 489 mobility relationship a mathematical parameter, the fractal dimension ( $D_f$ ), which is  
 490 approximately expressed as a power-law relationship between the mass of the  
 491 agglomerate particle ( $m$ ) and its mobility diameter ( $d_{mob}$ ), expressed as

$$492 \quad m = k \cdot d_{mob}^{D_{fm}} \quad (1)$$

493 where the prefactor  $k$  is a constant and  $D_{fm}$  is the mass-mobility scaling exponent, which  
 494 was sometimes erroneously called the ‘fractal dimension’ in previous studies (e.g., Park  
 495 et al., 2003). This quantity corresponds well to the virtual  $D_f$  and represents the  
 496 morphology of the BC aggregates (Sorensen, 2011). It should be noted that the  
 497 approximation is applied only when the  $D_f$  is greater than 2, the regime in which the  
 498 extBC particles are generally located (Park et al., 2003). The  $D_{fm}$  value of a sphere is 3.  
 499 Thus, the morphology of a particle is becomes increasingly closer and closer to that of  
 500 a sphere if as the  $D_{fm}$  increases gradually to 3.

501 The effective density ( $\rho_{eff}$ ) of the extBC particles is calculated as the ratio of the BC  
 502 mass ( $m$ ) measured using the SP2 and its the BC volume, which is based on the  
 503  $d_{mob}$  mobility diameter selected by the DMA, expressed as

$$504 \quad \rho_{eff} = \frac{6m}{\pi d_{mob}^3} \quad (2)$$

505 Combining Eq. 1 and 2,  $\rho_{eff}$  can also be expressed as a function of  $d_{mob}$ ,

$$506 \quad \rho_{eff} = K \cdot d_{mob}^{D_{fm}D_f - 3} \quad (3)$$

507 where  $K$  is a constant, corresponding to the prefactor  $k$  in the mass-mobility relationship.  
508 The dynamic shape factor is also calculated to indicate the morphology of the *extBC*  
509 particles. It is derived from the ratio of the slip-corrected mass-equivalent diameter  
510 ( $d_{me}$ ) and  $d_{mob}$ , expressed as

$$511 \chi = \frac{d_{mob} \cdot C_c(d_{me})}{d_{me} \cdot C_c(d_{mod})} \quad (4)$$

512 where  $d_{me}$  is calculated from the BC mass ( $m$ ) by assuming the BC particle to be a  
513 compact sphere with a density of  $1.8 \text{ g cm}^{-3}$  (Taylor et al., 2015), and  $C_c$  is the  
514 Cunningham slip correction factor parameterized by particle diameter ( $d$ )

$$515 C_c(d) = 1 + \frac{2\lambda}{d} [\alpha + \beta \exp(-\frac{\gamma \cdot d}{2\lambda})] \quad (5)$$

516 where  $\lambda$  is the mean free path of the gas molecules, which is set to 65 nm in this study  
517 according to Zhang et al. (2016). The values of the three empirical parameters  $\alpha$ ,  $\beta$  and  
518  $\gamma$  are 1.257, 0.4 and 1.1, respectively (Eq. 9.34 at on pPage 407 in Seinfeld and Pandis,  
519 2006).

## 520

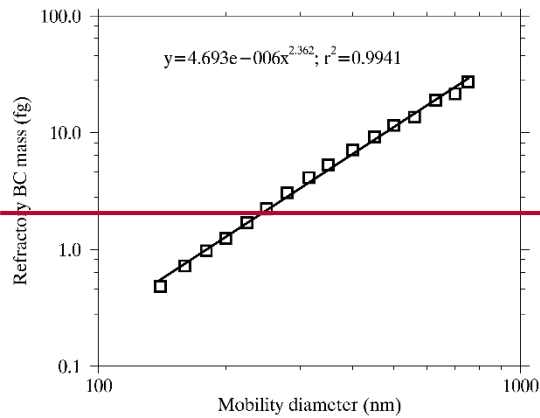
## 521 **4 Results and discussion**

### 522 **4.1 Fraactal dimensionMass-mobility relationship of the ambient *extBC***

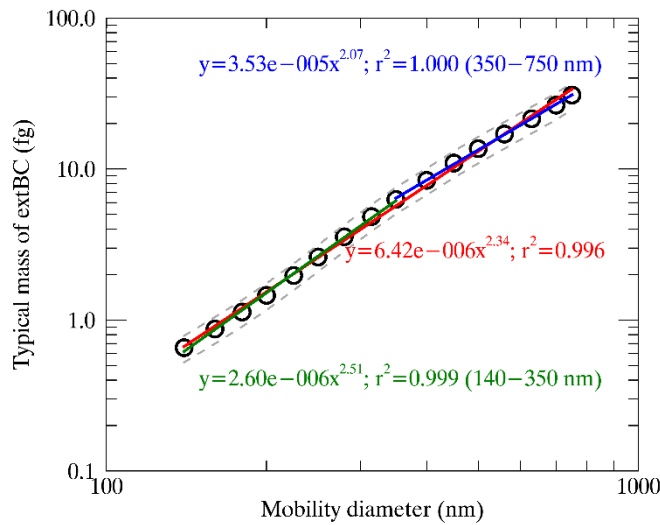
523 A ~~power-law~~ relationship was applied to the  $d_{mob}$ -determined *extBC* mass values,  
524 delivering the ~~fractal dimension~~mass-mobility scaling exponent ( $D_{fm}$ ) of the ambient  
525 *extBC* (Fig. 3). In the  ~~$d_{mob}$ mobility diameter~~ range of 140–750 nm, the fitted  $D_{fm}$  is  
526 2.3634, with one standard deviation of 0.0403. ~~It~~ The fitted  $D_{fm}$  is ~~comparable with~~close  
527 to the lower limit of the  $D_{fm}$  values of diesel exhaust particles presented in the literature,  
528 indicating the dominant contribution of diesel exhaust to the *extBC* in our measurement  
529 site in urban Beijing. ~~For example, d~~Depending on the fuel type, engine type and load,  
530 the  $D_{fm}$  of diesel exhaust particles measured by the DMA-APM or DMA-ELPI systems  
531 ranged between 2.22 and 2.84 (Park et al., 2003; Olfert et al., 2007; Maricq and Xu,  
532 2004; Olfert et al., 2007Park et al., 2003 and references therein). The higher  $D_{fm}$  values  
533 in the literature are likely attributed to the higher fraction of volatile and/or semivolatile  
534 components (e.g., sulfate) in the diesel exhaust (Park et al., 2003; Olfert et al., 2007).  
535 Accompanied by these volatile and/or semi-volatile components would result in a more

536 compact structure of the particle, leading to a higher  $D_{fm}$  value compared to the bare  
537 BC aggregate. This similarity indicates the dominant contribution of diesel exhausts to  
538 the  $extBC$  in our measurement site in urban Beijing. A high fraction of organic and/or  
539 inorganic (e.g., sulfate) components in the diesel exhausts increased the  $D_f$  values by  
540 filling in the gap of the chain like agglomerates or coatings outside the primary  
541 spherules (Park et al., 2003; Olfert et al., 2007). Since the rBC mass instead of the whole  
542 particle mass of  $extBC$  was measured by the SP2, the relatively low  $D_{fm}$  was expected  
543 and reasonable in this study. ThusIn addition, the relatively low  $D_{fm}D_f$  value observed  
544 in urban Beijing is also likely ~~related~~ to imply the high fuel quality (e.g., low sulfur  
545 content) and ~~more~~ efficient combustion in ~~the~~ vehicle engines, which decrease the  
546 organic and/or inorganic fractions in diesel exhaust particleless. The  $D_{fm}$  value for the  
547 ambient soot agglomerates measured with a DMA-APM system near a diesel truck-  
548 dominated highway was 2.41 (Geller et al., 2006), ~~very close to~~slightly higher than the  
549 value in our study.

550 According to Sorensen (2011), the ideal fractal-like DLCA with a virtual  $D_f$  of  
551 approximately 1.78 should have an expected  $D_{fm} \approx 2.2$  in the slip flow regime in which  
552 the BC aggregates are generally observed. The slightly larger  $D_{fm}$  value of ambient  
553  $extBC$  (2.34) in the current study might indicate a more compact structure than the ideal  
554 fractal-like DLCA due to the reconstruction effect by other components in the  
555 atmosphere. The reconstruction effect appears to be more significant in the smaller  
556 particle range than in the larger particle range. The smaller BC particles are more likely  
557 to be coated by volatile and/or semivolatile materials, which will be discussed in detail  
558 in the next section. We piecewise fitted the mass-mobility relationship using the power  
559 law function in the mobility ranges of 140–350 nm and 350–750 nm. A  $D_{fm}$  of  
560  $2.51 \pm 0.04$  that was obtained in the smaller mobility range (140–350 nm) was obviously  
561 larger than the fitted value in the whole size range (140–750 nm). In contrast, a much  
562 lower  $D_{fm}$  with value of  $2.07 \pm 0.02$  was observed in the larger mobility range (350–750  
563 nm). These results indicate that the ambient  $extBC$  particles with larger mobility  
564 diameters were likely less influenced by the reconstruction effect than those with  
565 smaller mobility diameters.



566



567

568 Fig. 3 The mass of *extBC* particles as a function of the mobility diameter in the range  
 569 of 140–750 nm (gray squares/black circles), fitted by a power-law relationship  
 570 (black-red line). The power law functions piecewise fitted in the 140–350 nm mobility  
 571 range (green line) range and in the 350–750 nm mobility range (blue line) are overlaid.  
 572 The dashed lines represent in the uncertainties in the determined *extBC* masses.

573

574 Table 1 The typical mass-equivalent diameters ( $d_{me}$ ) and corresponding masses of *extBC*  
 575 at different mobility sizes ( $d_{mob}$ ) selected by the DMA in the whole campaign, in a  
 576 polluted episode and in a clean period. The effective densities ( $\rho_{eff}$ ) and dynamic shape  
 577 factors ( $\chi$ ) at the  $d_{mob}$  selected by the DMA in the whole campaign are also presented.

$d_{mob}$ (nm)	$d_{me}$ (nm)			mass (fg)			$\rho_{eff}$ (g cm <sup>-3</sup> )	$\chi$
	total	polluted	clean	total	polluted	clean		
140	88.8	87.2	88.5	0.66	0.63	0.65	0.46	2.16
160	97.5	96.9	98.1	0.87	0.86	0.89	0.41	2.27
180	106.2	106.1	107.0	1.13	1.13	1.15	0.37	2.35

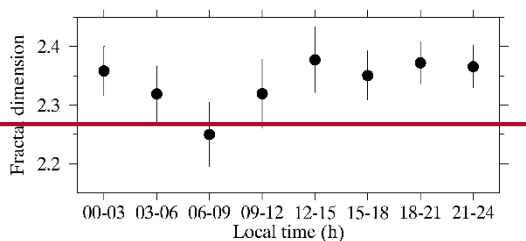
<u>200</u>	<u>115.6</u>	<u>116.1</u>	<u>115.5</u>	<u>1.46</u>	<u>1.48</u>	<u>1.45</u>	<u>0.35</u>	<u>2.40</u>
<u>225</u>	<u>127.9</u>	<u>128.6</u>	<u>128.4</u>	<u>1.97</u>	<u>2.01</u>	<u>1.99</u>	<u>0.33</u>	<u>2.41</u>
<u>250</u>	<u>140.5</u>	<u>142.2</u>	<u>141.0</u>	<u>2.62</u>	<u>2.71</u>	<u>2.64</u>	<u>0.32</u>	<u>2.41</u>
<u>280</u>	<u>155.8</u>	<u>158.0</u>	<u>154.4</u>	<u>3.56</u>	<u>3.72</u>	<u>3.47</u>	<u>0.31</u>	<u>2.41</u>
<u>315</u>	<u>172.6</u>	<u>174.8</u>	<u>170.6</u>	<u>4.85</u>	<u>5.04</u>	<u>4.68</u>	<u>0.30</u>	<u>2.40</u>
<u>350</u>	<u>188.2</u>	<u>191.8</u>	<u>185.9</u>	<u>6.28</u>	<u>6.65</u>	<u>6.05</u>	<u>0.28</u>	<u>2.41</u>
<u>400</u>	<u>207.4</u>	<u>213.7</u>	<u>207.4</u>	<u>8.41</u>	<u>9.20</u>	<u>8.41</u>	<u>0.25</u>	<u>2.43</u>
<u>450</u>	<u>226.4</u>	<u>232.3</u>	<u>225.9</u>	<u>10.94</u>	<u>11.81</u>	<u>10.87</u>	<u>0.23</u>	<u>2.50</u>
<u>500</u>	<u>243.8</u>	<u>251.4</u>	<u>242.2</u>	<u>13.65</u>	<u>14.98</u>	<u>13.39</u>	<u>0.21</u>	<u>2.62</u>
<u>560</u>	<u>262.6</u>	<u>271.1</u>	<u>260.1</u>	<u>17.06</u>	<u>18.77</u>	<u>16.58</u>	<u>0.19</u>	<u>2.71</u>
<u>630</u>	<u>283.2</u>	<u>293.5</u>	<u>282.5</u>	<u>21.42</u>	<u>23.83</u>	<u>21.25</u>	<u>0.16</u>	<u>2.81</u>
<u>700</u>	<u>305.1</u>	<u>312.7</u>	<u>305.0</u>	<u>26.76</u>	<u>28.83</u>	<u>26.73</u>	<u>0.15</u>	<u>2.89</u>
<u>750</u>	<u>319.6</u>	<u>328.8</u>	<u>323.5</u>	<u>30.76</u>	<u>33.49</u>	<u>31.92</u>	<u>0.14</u>	<u>2.93</u>

578

579 Fig. 4 shows the diurnal variation of  $D_f$ . A significant low value of  $D_f$  ( $2.25 \pm 0.05$ ) was  
580 observed in the morning traffic rush hours (06:00–09:00 local time). Freshly emitted  
581 *extBC* particles from vehicle exhaust have a looser chain-like structure corresponding  
582 to a low  $D_f$  value. The highest  $D_f$  value ( $2.38 \pm 0.06$ ) in the afternoon (12:00–15:00 local  
583 time) is likely related to the aging processes of the *extBC* particles in the ambient  
584 atmosphere. Aging processes not only result in a higher fraction of *intBC* particles (Wu  
585 et al., 2016, 2017) but they can also lead to a more compact structure of *extBC* particles,  
586 and in turn, a higher  $D_f$  value. BC particles thinly coated by organic/inorganic  
587 components were somewhat considered as *extBC* using the SP2 time delay approach  
588 (Moteki and Kondo, 2007; Laborde et al., 2012). However, less mass condensed onto  
589 the BC primary particles would lead to more compaction of the *extBC* particles even  
590 when the  $d_{\text{mob}}$  remained constant (Slowik et al., 2007).

591 The variation in the morphology of *extBC* was further examined by comparing the  
592 mass-mobility relationship in a polluted episode and in a consecutively clean period.  
593 As shown in Fig. S7, a polluted episode rapidly formed at 14:00 (local time, if not  
594 specified) on 26 January and lasted one and a half days to 0:00 on 28 January 2018.  
595 The mean  $\text{PM}_{2.5}$  mass concentration was  $72.1 \pm 23.1 \mu\text{g m}^{-3}$  in this polluted episode,  
596 three times the campaign average value ( $23.0 \pm 26.7 \mu\text{g m}^{-3}$ ). The  $D_{\text{fm}}$  value is  $2.42 \pm 0.09$   
597 in the polluted episode, higher than that ( $2.33 \pm 0.06$ ) observed in the consecutively clean  
598 period from 1:00 on 28 January to 18:00 on 31 January 2018, during which the average

599 PM<sub>2.5</sub> concentration was merely 8.9±2.7 μg m<sup>-3</sup> (Fig. S8). The higher  $D_{fm}$  in the polluted  
 600 episode is mainly due to the increase in the masses of *extBC* at large mobility sizes (e.g.,  
 601  $d_{mob} > 250$ ). As shown in Table 1, the typical masses of *extBC* in the 280–700 nm  $d_{mob}$   
 602 range in the polluted episode are ~7–13% larger than those in the clean period.  
 603 Although the differences might result from the uncertainty (~20%) in the mass  
 604 determination of *extBC*, the commonly larger *extBC* masses (in the 280–700 nm  $d_{mob}$   
 605 range) to some degree still imply a possibly more compact structure of *extBC*  
 606 aggregates in the polluted episode, which might relate to changes in the dominant  
 607 sources and the ambient environment. Previous studies have revealed that regionally  
 608 transported pollutants emitted from coal combustion and/or biomass burning played an  
 609 important or even predominant role in polluted episodes in Beijing (Wu et al., 2017;  
 610 Ma et al., 2017a). Thus, a considerable fraction of *extBC* aggregates from these sources  
 611 is likely to coexist with the local vehicle-emitted BC aggregates in the polluted episode,  
 612 even though the proportion of *extBC* in the total BC-containing particles decreased (Fig.  
 613 S9). These transported BC aggregates originating from coal combustion and/or biomass  
 614 burning might have a more compact structure than those from vehicle exhaust due to  
 615 the differences in the combustion environments and efficiencies. In addition, the BC  
 616 aggregates might also become more compact due to the reconstruction effect by the  
 617 volatile and/or semivolatile components which are generally abundant in polluted  
 618 episodes. Both possible factors are likely to result in the larger  $D_{fm}$  values in the polluted  
 619 episode.



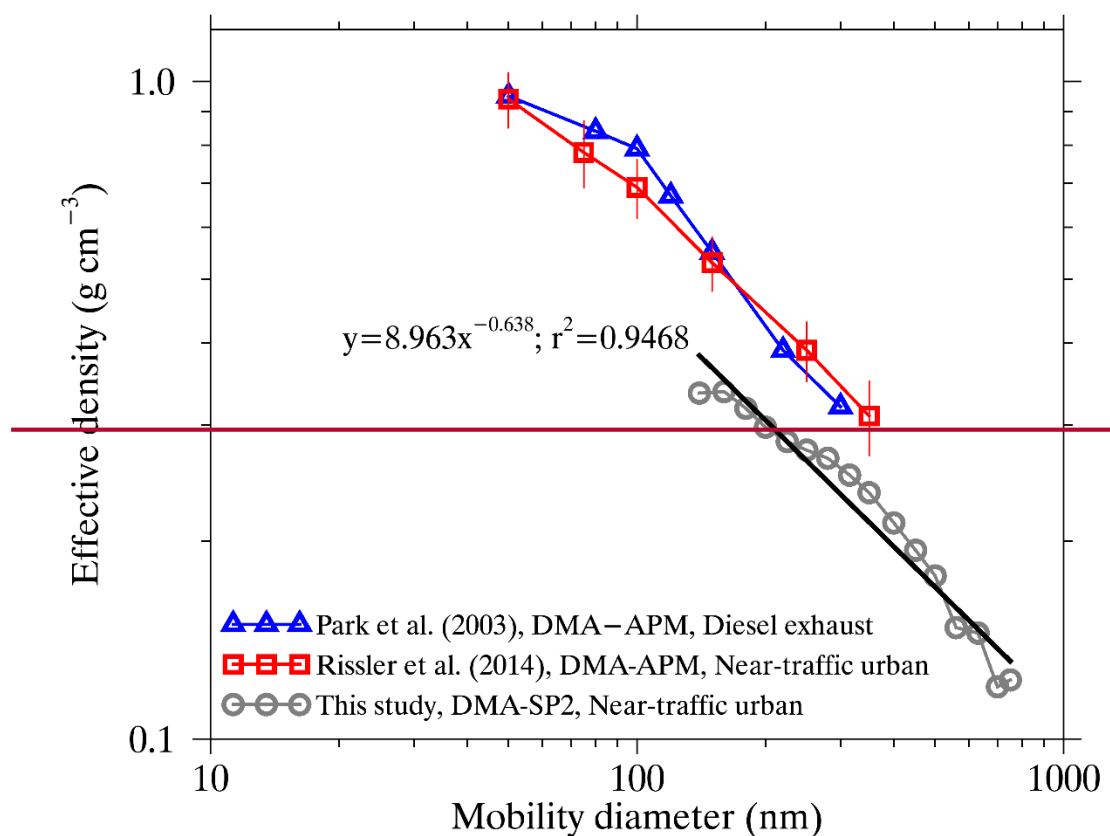
620  
 621 ~~Fig. 4 The diurnal variation of the fractal dimension ( $D_f$ ) of ambient *extBC* particles.~~  
 622 ~~The error bars represent one standard deviation of the fitted  $D_f$ .~~

623

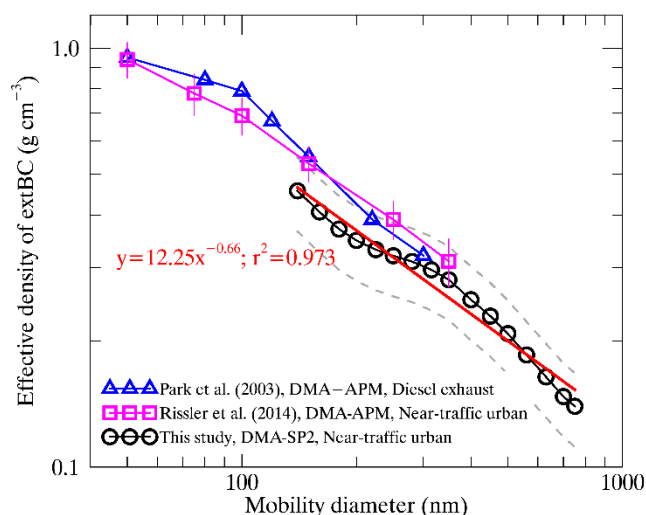
## 624 4.2 Size-resolved effective densities of the ambient *extBC*

625 In contrast to the mass of *extBC* ( $m$ ), the effective density of the *extBC* particles ( $\rho_{eff}$ )

626 showed a significant decreasing trend as the  $d_{\text{mob}}$  increased from 140 nm to 750 nm  
 627 (Fig. 54 and Table 1). The highest  $\rho_{\text{eff}}$  of 0.34–46 g cm<sup>-3</sup> was observed in the 140 nm  
 628  $d_{\text{mob}}$  ~~range of 140–160 nm~~, likely ~~due to~~ because the BC aggregates at the smallest size  
 629 are made up of the fewest primary spherules ~~of the BC aggregates at the smallest size~~.  
 630 When the  $d_{\text{mob}}$  increased to 700–750 nm,  $\rho_{\text{eff}}$  decreased to as low as 0.12–14 g cm<sup>-3</sup>,  
 631 approximately one-third of that at 140–160 nm. The very low  $\rho_{\text{eff}}$  values agree well with  
 632 the fractal-like nature of the *ext*BC particles.



633



634

635 Fig. 5.4 The effective density ( $\rho_{\text{eff}}$ ) of the *extBC* particles as a function of the mobility  
 636 diameter ( $d_{\text{mob}}$ ) (gray-black eyescircles). The black-red line represents the power  
 637 power-law fitting of  $\rho_{\text{eff}}$  against  $d_{\text{mob}}$ . The variations of  $\rho_{\text{eff}}$  with  $d_{\text{mob}}$  measured for the  
 638 soot agglomerates from diesel exhausts (Park et al., 2003) and near-traffic urban  
 639 environments (Rissler et al., 2014) are also presented as blue triangles and red squares,  
 640 respectively. The dashed lines represent in the uncertainties in the determined  $\rho_{\text{eff}}$ .

641

642 The  $\rho_{\text{eff}}$  values measured-withobtained by the DMA-SP2 measurements are  
 643 considerably lower than those close to those of the lower limits of diesel exhaust  
 644 particles measured by the DMA-APM (or CPMA) or DMA-ELPI systems. Park et al.  
 645 (2003) reported a decrease in the  $\rho_{\text{eff}}$  of diesel exhaust particles under a moderate (50%)  
 646 engine load from  $0.95 \text{ g cm}^{-3}$  to  $0.32 \text{ g cm}^{-3}$  as the mobility diameter increased from 50  
 647 nm to 300 nm (Fig. 5.4). The  $\rho_{\text{eff}}$  values presented in Park et al. (2003) are approximately  
 648 1.62-1.25, 1.34-1.18 and 1.23-1.05 times those in our study at ~150 nm, 220 and 300 nm  
 649 in mobility diameter, respectively. The differences in  $\rho_{\text{eff}}$  values between our study and  
 650 the literature are generally within the uncertainty (~20%) in the mass determination of  
 651 *extBC* at prescribed mobility sizes. However, the commonly lower  $\rho_{\text{eff}}$  values are also  
 652 likely due to the techniques used to determine the mass of BC aggregates. Some  
 653 previous studies on the  $\rho_{\text{eff}}$  of diesel exhaust particles using the DMA-APM or DMA-  
 654 ELPI tandem measurements also commonly showed a slightly larger  $\rho_{\text{eff}}$  throughout the  
 655 comparable mobility ranges (e.g., ~150–350 nm) than that measured in this study

656 (Maricq and Xu, 2004; Olfert et al., 2007). The masses of the bare BC particles were  
657 determined by the laser-induced incandescence technique of the SP2. In a previous  
658 tandem system, the APM (or CPMA) or ELPI was utilized to determine the typical  
659 mass of BC aggregates at a given mobility, and the BC aggregates are likely composed  
660 of a fraction of volatile and/or semivolatile components in addition to the bare primary  
661 particles. These volatile and/or semivolatile components increase the mass of the whole  
662 particle, resulting in a larger  $\rho_{\text{eff}}$  value at a certain mobility and cause a compact  
663 structure of the BC aggregate. Nevertheless, the  $\rho_{\text{eff}}$  values reported in the literature also  
664 differ. For example, Olfert et al. (2007) found that the  $\rho_{\text{eff}}$  of diesel exhaust particles  
665 coated with ~~little-minor~~ sulfate and water contents ( $\sim 2\%$  of the total particle mass) was  
666  $\sim 0.4 \text{ g cm}^{-3}$  at 299 nm, only slightly larger than the value of diesel exhaust particles  
667 ( $0.32 \text{ g cm}^{-3}$ ) measured in Park et al. (2003) and ~~0.26~~ that of extBC in the urban  
668 atmosphere ( $0.31 \text{ g cm}^{-3}$ ) in our study ~~for at~~ the same mobility size. However, the  $\rho_{\text{eff}}$   
669 value increased significantly to  $\sim 0.71 \text{ g cm}^{-3}$  at a relatively high engine load of 40%  
670 due to the high sulfate levels ( $\sim 30\%$  of the total particle mass) in the diesel exhaust  
671 particles (Olfert et al., 2007).

672 The  $\rho_{\text{eff}}$  of ambient soot aggregates also showed a similar decreasing trend with  
673 increasing  $d_{\text{mob}}$  based on the DMA-APM system (Geller et al., 2006; Rissler et al.,  
674 2014). Rissler et al. (2014) showed a decrease in the average  $\rho_{\text{eff}}$  of BC aggregates from  
675  $0.94 \text{ g cm}^{-3}$  to  $0.31 \text{ g cm}^{-3}$  in the near-traffic urban environment as the  $d_{\text{mob}}$  increased  
676 from 50 nm to 350 nm (Fig. 54), similar to that of the freshly emitted diesel exhaust  
677 particles presented in Park et al. (2003). However, based on the same method, the  $\rho_{\text{eff}}$   
678 values of the ambient BC aggregates that mostly originated from diesel exhausts (Geller  
679 et al., 2006) are ~~largely-substantially~~ different from those presented in Rissler et al.  
680 (2014), especially in the large particle size range. The  $\rho_{\text{eff}}$  at  $\sim 350 \text{ nm}$  was  $0.17 \text{ g cm}^{-3}$   
681 in Geller et al. (2006), approximately half of the value presented in Rissler et al. (2014).  
682 The reason for the discrepancy might be related to the large measurement uncertainties  
683 of the DMA-APM system for large particles, e.g., with sizes greater than 300 nm in the  
684  $d_{\text{mob}}$ , since these large particles are less abundant in the ambient atmosphere (Geller et  
685 al., 2006). Compared to the results presented in Rissler et al. (2014), the  $\rho_{\text{eff}}$  values of

686 ambient *extBC* aggregates in our study are slightly lower, e.g., by ~17%, ~18% and ~6%  
687 in 150 nm, 250 nm and 350 nm  $d_{mob}$ , respectively. The relatively higher  $\rho_{eff}$  values are  
688 also likely attributed to the effects of volatile and/or semivolatile components in the  
689 soot aggregates. Rissler et al. (2014) found that the residual volatile-mass fraction of  
690 volatile and/or semivolatile materials in the soot aggregates was ~10%, whenever  
691 when the sample air was heated to 300 °C before entering the system for measurement.  
692 It is interesting to note that the  $\rho_{eff}$  values appear to be closer to the values presented in  
693 the literature using the DMA-APM measurements in the 280–350 nm  $d_{mob}$  range (Fig.  
694 4). As shown in Fig. 3, larger typical masses of *extBC* in this range are also observed  
695 beyond the logarithmic scaled linear curve that is fitted to the mass-mobility  
696 relationship. The relatively larger masses and  $\rho_{eff}$  values might imply a more compact  
697 structure of *extBC* aggregates in this range which is likely resulted from the  
698 reconstruction effect by the ambient volatile and/or semivolatile components. As shown  
699 in Fig. S9, the size-resolved number fractions of *extBC* exhibit a minimum in the 280–  
700 350 nm  $d_{mob}$  regardless of whether they are associated with the polluted episode or the  
701 clean period. This finding indicates that particles in this mobility range are more likely  
702 to be thickly coated by other components compared to those in the smaller or larger  
703 mobility ranges. Zhang et al. (2016) also observed an increased coating thickness of the  
704 BC-containing particles in the mobility range of 200–350 nm (Table 1 in the literature)  
705 using the VTDMA-SP2 measurement at a suburban site ~70 km away from our  
706 observation site, although the variation in the coating thickness in the larger mobility  
707 range was not investigated. It should be noted that the number fraction of *extBC* at each  
708 mobility size presented in Fig. S9 is roughly calculated as the ratio of the *extBC* number  
709 concentration to the sum of *extBC* and *intBC*, in which the multiply charged effects  
710 were not corrected. Although the *extBC* particles without and/or with thin coatings are  
711 the focus of the current study, the higher fraction of thickly coated BC particles in the  
712 280–350 nm  $d_{mob}$  range implies a higher possibility that these *extBC* particles in the  
713 same range were affected by volatile and/or semivolatile materials in the atmosphere,  
714 in turn resulting in a more compact structure of these BC aggregates. Further detailed  
715 studies of the size distribution of BC (including *extBC*, *intBC* and both) and non-BC

716 particles based on the combined measurements of SP2 and CPC are needed in our  
717 further work to reveal the potential mechanism for this phenomenon.

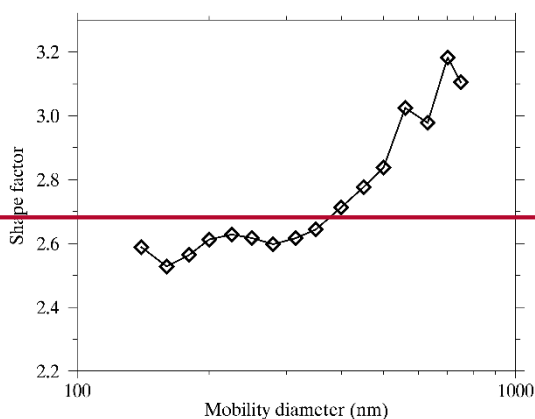
718 ~~The DMA-APM system directly measures the mass of particles selected at a given~~  
719 ~~mobility diameter by the DMA. The organic and/or inorganic components filling in the~~  
720 ~~gap or coating outside the primary spherules will increase the mass of the BC~~  
721 ~~agglomerates, although their content might not be significant in fresh exhausts. Olfert~~  
722 ~~et al. (2007) showed that sulfates and water accounted for ~2% of the mass of the total~~  
723 ~~particulate matter under a low engine load (15%) and increased to ~30% under a high~~  
724 ~~engine load (40%). Rissler et al. (2014) found that the volatile mass fraction of the soot~~  
725 ~~aggregate was ~10% when heated to 300 °C. Thus, in practice, the DMA-APM system~~  
726 ~~measured the  $\rho_{\text{eff}}$  of soot particles comprising chain-like BC aggregates and a few~~  
727 ~~volatile components instead of pure BC. However, the SP2 measured the mass of pure~~  
728 ~~BC merely through its incandescence in the laser beam, and the DMA-SP2 system~~  
729 ~~determined the  $\rho_{\text{eff}}$  of *ext*BC exclusive of those volatile components coupled in the BC~~  
730 ~~particles. Thus, a lower  $\rho_{\text{eff}}$  was obtained, but this value was likely closer to the value~~  
731 ~~of the pure *ext*BC particles.~~

732 Although the  $\rho_{\text{eff}}$  of *ext*BC at small sizes ( $d_{\text{mob}} < 140$  nm) cannot be determined due to  
733 the lower limitation of the DMA-SP2 system, we extended the  $\rho_{\text{eff}}$  of *ext*BC to a large  
734 size range ( $300 < d_{\text{mob}} < 750$  nm), which was barely investigated in previous studies  
735 using tandem measurements. A continuous decrease in  $\rho_{\text{eff}}$  with increasing  $d_{\text{mob}}$  was  
736 observed even in the large size range between 300-350 nm and 750 nm (Fig. 54). It is  
737 reasonable to infer that the structure of the *ext*BC particles is-becomes looser when the  
738 agglomerate-chainfractal-like aggregates built up by the primary spherules increases.

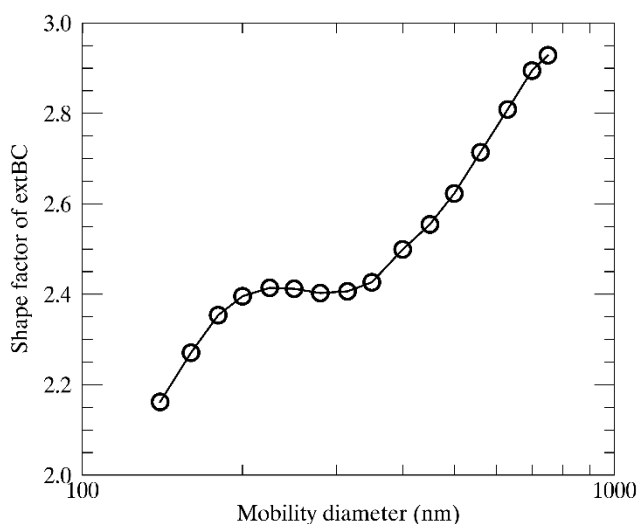
#### 740 **4.3 Dynamic shape factors of the ambient *ext*BC**

741 Due to their chainfractal-like structures, the *ext*BC particles generally have large  
742 dynamic shape factors ( $\chi$ ) with values in the range of 2.53-16 to 3.182.93 (Table 1),  
743 much larger than ~~that those~~ of *int*BC with an average value of ~1.2 (Zhang et al., 2016).  
744 The  $\chi$  value declined exponentially as a function of coating thickness of BC-containing  
745 particles (Zhang et al., 2016). In general, the  $\chi$  values are significantly higher for larger

746 particle sizes. In contrast to the decrease in  $\rho_{\text{eff}}$ , the  $\chi$  values of *extBC* generally increase  
 747 as the  $d_{\text{mob}}$  increases from 140 nm to 750 nm (Fig. 5). The *extBC* particles 700–750 nm  
 748 in mobility diameter have a mean  $\chi$  value of 3.182.93, approximately 1.26–36 times that  
 749 for 160–140 nm  $d_{\text{mob}}$  particles (Table 1). The larger particles have longer chains and  
 750 looser structures, resulting in higher  $\chi$  values. However, the  $\chi$  values appear to varied  
 751 vary slightly, fluctuating in a narrow range between 2.53–40 to 2.64–41 in the size range  
 752 of 140–200 nm to 350 nm (Fig. 5). The hiatus in the gradual increase in  $\chi$  should also  
 753 relate to the more compact structure of *extBC* particles in the 280–350 nm mobility  
 754 range, which has been discussed in detail in the previous sections. This is attributed to  
 755 the large drag force for smaller particles.



756



757

758 Fig. 6-5 The dynamic shape factor of the *extBC* particles as a function of the mobility  
 759 diameter in the range of 140–750 nm.

760

761 **5 Conclusions**

762 The DMA-SP2 system was established to study the morphology and effective density  
 763 of the ambient *extBC* particles, especially in the larger mobility size range, i.e.,  
 764 350< $d_{\text{mob}}$ <750 nm, which was seldom investigated in previous tandem measurements.  
 765 ~~The q~~Quasi-monodisperse particles in the  $d_{\text{mob}}$  range of 20–750 nm were stepwise  
 766 selected using the DMA and then delivered to the SP2 for rBC mass measurement and  
 767 mixing state discrimination. The time difference between the size selection and the SP2  
 768 measurement was previously processed using the local peak approach. The normalized  
 769 number size distribution of *extBC*, distinguished as having a delay time between the  
 770 incandescence signal peak and the scattering peak detected by the SP2 of less than 2  $\mu\text{s}$ ,  
 771 as a function of  $d_{\text{me}}$  was investigated at each prescribed mobility size in the range of  
 772 140–750 nm. The size distributions at smaller mobility sizes were not presented due to  
 773 the lower limit of the rBC mass determined by using the SP2. The peak  $d_{\text{me}}$ , calculated  
 774 as the mode value of a lognormal function fitted to the major peak of the size  
 775 distribution, was determined as the typical  $d_{\text{me}}$  value at each mobility size. Consequently,  
 776 the typical mass of *extBC* at each mobility size was identified. Reducing the delay time  
 777 threshold employed to discriminate the *extBC* had few effects on the determined masses  
 778 of *extBC*, implying the reliability of our study for the *extBC* particles. The uncertainty  
 779 in the determined *extBC* masses was ~20%, combining the uncertainty in the SP2-  
 780 measured rBC mass with that related to the time-delay approach.~~Gaussian fitting was~~  
 781 ~~performed to the *extBC* mass frequency distribution to minimize the effect of~~  
 782 ~~multicharged particles and obtain the typical *extBC* mass at a given  $d_{\text{mob}}$ .~~ On this basis,  
 783 the mass-mobility relationship of ambient *extBC* in urban Beijing was investigated.  
 784 ~~†~~The campaign average  $D_{\text{fm}}$  value was estimated to be 2.3634±0.0403 by fitting the  
 785 derived *extBC* masses ~~against~~ as a power-law function of  $d_{\text{mob}}$  in the range of 140–750  
 786 nm, close to the lower-limit  $D_{\text{fm}}$  ~~$D_{\text{f}}$~~  values of diesel exhaust particles. A relatively ~~lower~~  
 787 larger  $D_{\text{f}}$  value was observed in the ~~morning traffic rush hours~~polluted episode than in  
 788 the clean period (2.42±0.09 vs. 2.33±0.06), implying a ~~–~~ more compact structure of BC  
 789 aggregates in the polluted episode~~significant contribution of vehicle emissions to the~~  
 790 ~~agglomerate BC particles.~~–

791 A decrease in  $\rho_{\text{eff}}$  with increasing  $d_{\text{mob}}$  was observed, with the  $\rho_{\text{eff}}$  value decreasing from

792 0.34–46 g cm<sup>-3</sup> at 140–160 nm mobility to 0.12–14 g cm<sup>-3</sup> at 700 nm. The  $\rho_{\text{eff}}$  values  
793 derived using the DMA-SP2 measurement were generally slightly lower than those  
794 based on the DMA-APM measurement. This difference was most likely due to the bias  
795 in the *ext*BC mass determination between using the SP2 and APM techniques. The pure  
796 refractory-rBC mass determined using the SP2 in this study was generally lower than  
797 the total mass of the BC aggregate, which comprises both refractory-rBC and a possible  
798 fraction of nonrefractory organic and/or inorganic components. The  $\rho_{\text{eff}}$  values in the  
799 280–350 nm mobility range appeared to be much closer to the values for soot  
800 aggregates reported in the literature by using the DMA-APM tandem measurement.  
801 This finding might be related to the more compact structure of BC aggregates in this  
802 range, which was likely influenced by the reconstruction effect of volatile and/or  
803 semivolatile components in the atmosphere. The reconstruction effect might also result  
804 in a hiatus in the gradually increased  $\chi$  value in the range of 200–350 nm. The large  $\chi$   
805 values varying in the range of 2.53 to 3.18 were derived. Large  $\chi$  values generally  
806 increased from 2.16 to 2.93 with increasing  $d_{\text{mob}}$  at different  $d_{\text{mob}}$ , further implying the  
807 high fractal structure of *ext*BC particles.

808

## 809 **Acknowledgements**

810 This work was supported by the National Key Research and Development Program of  
811 China (no. 2017YFC0209601, 2017YFC0212701) and the National Natural Science  
812 Foundation of China (no. 41575150, 41775155, 91644217 and 91644219).

813

## 814 **References**

- 815 Alexander, D. T., Crozier, P. A., and Anderson, J. R.: Brown carbon spheres in East Asian outflow and their optical  
816 properties, *Science*, 321, 833–836, doi:10.1126/science.1155296, 2008.
- 817 Bi, L., Yang, P., Kattawar, G. W., Mishchenko, M. I.: Efficient implementation of the invariant imbedding T-matrix  
818 method and the separation of variables method applied to large nonspherical inhomogeneous particles, *J. Quant.*  
819 *Spectrosc. Radiat. Transfer*, 116, 169–183, doi:10.1016/j.jqsrt.2012.11.014, 2013.
- 820 Huang, R. J., Zhang, Y. L., Bozzetti, C., Ho, K.-F., Cao, J. J., Han, Y. M., Daellenbach, K. R., Slowik, J. G., et al.:  
821 High secondary aerosol contribution to particulate pollution during haze events in China, *Nature*, 514, 218–222,  
822 doi:10.1038/nature13774, 2014.
- 823 Huang, X. F., Sun, T. L., Zeng, L. W., Yu, G. H., and Luan, S. J.: Black carbon aerosol characterization in a coastal  
824 city in South China using a single particle soot photometer, *Atmos. Environ.*, 51, 21–28,

825 doi:10.1016/j.atmosenv.2012.01.056, 2012.

826 [Gao, R. S., Schwarz, J. P., Kelly, K. K., Fahey, D. W., Watts, L. A., Thompson, T. L., Spackman, J. R., Slowik, J.](#)  
827 [G., Cross, E. S., Han, J.-H., Davidovits, P., Onasch, T. B., and Worsnop, D. R.: A novel method for estimating](#)  
828 [light-scattering properties of soot aerosols using a modified single-particle soot photometer, \*Aerosol Sci.\*](#)  
829 [Technol., 41, 125–135, doi:10.1080/02786820601118398, 2007.](#)

830 Geller, M., Biswas, S., and Sioutas, C.: Determination of particle effective density in urban environments with a  
831 differential mobility analyzer and aerosol particle mass analyzer, *Aerosol Sci. Technol.*, 40, 709–723,  
832 doi:10.1080/02786820600803925, 2006.

833 Gysel, M., Laborde, M., Olfert, J. S., Subramanian, R., and Gröhn, A. J.: Effective density of Aquadag and fullerene  
834 soot black carbon reference materials used for SP2 calibration, *Atmos. Meas. Tech.*, 4, 2851–2858,  
835 doi:10.5194/amt-4-2851-2011, 2011.

836 [Gysel, M., Laborde, M., Mensah, A. A., Corbin, J. C., Keller, A., Kim, J., Petzold, A., and Sierau, B.: Technical](#)  
837 [Note: The single particle soot photometer fails to reliably detect PALAS soot nanoparticles, \*Atmos. Meas.\*](#)  
838 [Tech., 5, 3099–3107, doi: 10.5194/amt-5-3099-2012, 2012.](#)

839 IPCC: Summary for policymakers, in: *Climate Change 2013: The Physical Science Basis. Contribution of Working*  
840 *Group I to the Fifth Assessment Report of the Intergovernmental Panel on Climate Change*, edited by: Stocker,  
841 T. F., Qin, D., Plattner, G.-K., Tignor, M., Allen, S. K., Boschung, J., Nauels, A., Xia, Y., Bex, V., and Midgley,  
842 P. M., Cambridge University Press, Cambridge, United Kingdom and New York, NY, USA, 2013.

843 Jacobson, M. Z.: Strong radiative heating due to the mixing state of black carbon in atmospheric aerosols, *Nature*,  
844 409, 695–697, doi:10.1038/35055518, 2001.

845 Khalizov, A. F., Xue, H. X., Wang, L., Zheng, J., and Zhang, R. Y.: Enhanced light absorption and scattering by  
846 carbon soot aerosol internally mixed with sulfuric acid, *J. Phys. Chem. A*, 113, 1066–1074, 2009.

847 Laborde, M., Mertes, P., Zieger, P., Dommen, J., Balternsperger, U., and Gysel, M.: Sensitivity of the Single Particle  
848 Soot Photometer to different black carbon types, *Atmos. Meas. Tech.*, 5, 1031–1043, doi:10.5194/amt-5-1031-  
849 2012, 2012.

850 [Liu, D., Allan, J., Whitehead, J., Young, D., Flynn, M., Coe, H., McFiggans, G., Fleming, Z. L., and Bandy, B.:](#)  
851 [Ambient black carbon particle hygroscopic properties controlled by mixing state and composition, \*Atmos.\*](#)  
852 [Chem. Phys., 13, 2015–2029, doi:10.5194/acp-13-2015-2013, 2013.](#)

853 Liu, D. T., Whitehead, J., Alfarra, M. R., Reyes-Villegas, E., Spracklen, D. V., Reddington, C. L., Kong, S. F.,  
854 Williams, P. I., Ting, Y.-C., Haslett, S., Taylor, J. W., Flynn, M. J., Morgan, W. T., McFiggans, G., Coe, H., and  
855 Allan, J. D.: Black-carbon absorption enhancement in the atmosphere determined by particle mixing state,  
856 *Nature Geoscience*, 10, 184–188, doi:10.1038/NGEO2901, 2017.

857 [Ma, Q. X., Wu, Y. F., Zhang, D. Z., Wang, X. J., Xia, Y. J., Liu, X. Y., Tian, P., Han, Z. W., Xia, X. A., Wang, Y., and](#)  
858 [Zhang, R. J.: Roles of regional transport and heterogeneous reactions in the PM<sub>2.5</sub> increase during winter haze](#)  
859 [episodes in Beijing, \*Sci. Tot. Environ.\*, 599–600, 246–253, doi:10.1016/j.scitotenv.2017.04.193, 2017a.](#)

860 [Ma, Q. X., Wu, Y. F., Tao, J., Xia, Y. J., Liu, X. Y., Zhang, D. Z., Han, Z. W., Zhang, X. L., and Zhang, R. J.:](#)  
861 [Variations of chemical composition and source apportionment of PM<sub>2.5</sub> during winter haze episodes in Beijing,](#)  
862 [Aerosol Air Qual. Res., 17, 2791–2803, doi:10.4209/aaqr.2017.10.0366, 2017b.](#)

863 Maricq, M. M., and Xu, N.: The effective density and fractal dimension of soot particles from premixed flames and  
864 motor vehicle exhaust, *J. Aerosol Sci.*, 35, 1251–1274, doi:10.1016/j.jaerosci.2004.05.002, 2004.

865 McMeeking, G. R., Good, N., Petters, M. D., McFiggans, G., and Coe, H.: Influences on the fraction of hydrophobic  
866 and hydrophilic black carbon in the atmosphere, *Atmos. Chem. Phys.*, 11, 5099–5112, doi:10.5194/acp-11-  
867 5099-2011, 2011.

868 Moteki, N. and Kondo, Y.: Effects of mixing state on black carbon measurements by laser-induced incandescence,

869 Aerosol Sci. Technol., 41, doi:10.1080/02786820701199728, 398–417, 2007.

870 Ning, Z., Chan, K. L., Wong, K. C., Westerdahl, D., Močnik, G., Zhou, J. H., Cheung, C. S.: Black carbon mass size  
871 distributions of diesel exhaust and urban aerosols measured using differential mobility analyzer in tandem with  
872 Aethalometer, *Atmos. Environ.*, 80, 31–40, doi:10.1016/j.atmosenv.2013.07.037, 2013.

873 Olfert, J. S., Symonds, J. P. R., and Collings, N.: The effective density and fractal dimension of particles emitted  
874 from a light-duty diesel vehicle with a diesel oxidation catalyst, *J. Aerosol Sci.*, 38, 69–82,  
875 doi:10.1016/j.jaerosci.2006.10.002, 2007.

876 Pagels, J., Khalizov, A. F., McMurry, P. H., and Zhang, R. Y.: Processing of soot by controlled sulphuric acid and  
877 water condensation—mass and mobility relationship, *Aerosol Sci. Technol.*, 43, 629–640,  
878 doi:10.1080/02786820902810685, 2009.

879 Park, K., Cao, F., Kittelson, D. B., and McMurry, P. H.: Relationship between particle mass and mobility for diesel  
880 exhaust particles, *Environ. Sci. Technol.*, 37, 577–583, doi:10.1021/es025960v, 2003.

881 Park, K., Kittelson, D. B., and McMurry, P. H.: Structural properties of diesel exhaust particles measured by  
882 transmission electron microscopy (TEM): relationships to particle mass and mobility, *Aerosol Sci. Technol.*,  
883 38, 881–889, doi:10.1080/027868290505189, 2004.

884 Park, K., Dutcher, D., Emery, M., Pagels, J., Sakurai, H., Scheckman, J., Qian, S., Stolzenburg, M. R., Wang, X.,  
885 Yang, J., and McMurry, P. H.: Tandem measurements of aerosol properties—a review of mobility techniques  
886 with extensions, *Aerosol Sci. Technol.*, 42, 801–816, doi:10.1080/02786820802339561, 2008.

887 Peng, J. F., Hu, M., Guo, S., Du, Z. F., Zheng, J., Shang, D. J., Zamora, M. L., Zeng, L. M., Shao, M., Wu, Y.-S.,  
888 Zheng, J., Wang, Y., Glen, C. R., Collins, D. R., Molina, M. J., and Zhang, R. Y.: Markedly enhanced absorption  
889 and direct radiative forcing of black carbon under polluted urban environments, *Proc. Natl. Acad. Sci. USA*,  
890 113, 4266–4271, doi:10.1073/pnas.1602310113, 2016.

891 [Raatikainen, T., Brus, D., Hooda, R. K., Hyvärinen, A.-P., Asmi, E., Sharma, V. P., Arola, A., and Lihavainen, H.:](#)  
892 [Size-selected black carbon mass distributions and mixing state in polluted and clean environments of northern](#)  
893 [India, \*Atmos. Chem. Phys.\*, 17, 371–383, doi:10.5194/acp-17-371-2017, 2017.](#)

894 Rissler, J., Nordin, E. Z., Eriksson, A. C., Nilsson, P. T., Frosch, M., Sporre, M. K., Wierzbicka, A., Svenningsson,  
895 B., Löndahl, J., Messing, M. E., Sjogren, S., Hemmingsen, J. G., Loft, S., Pagels, J. H., and Swietlicki, E.:  
896 Effective density and mixing state of aerosol particles in a near-traffic urban environment, *Environ. Sci.*  
897 *Technol.*, 48, 6300–6308, doi:10.1021/es5000353, 2014.

898 Seinfeld, J. H., and Pandis, S. N.: Atmospheric chemistry and physics, Chapter 9—Dynamics of single aerosol  
899 particles, John Wiley & Sons, Inc., Hoboken, New Jersey, 2006.

900 [Scarnato, B. V., Vahidinia, S., Richard, D. T., Kirchstetter, T. W.: Effects of internal mixing and aggregate](#)  
901 [morphology on optical properties of black carbon using a discrete dipole approximation model, \*Atmos. Chem.\*](#)  
902 [Phys., 13, 5089–5101, doi:10.5194/acp-13-5089-2013, 2013.](#)

903 Schwarz, J. P., Gao, R. S., Fahey, D. W., Thomson, D. S., Watts, L. A., Wilson, J. C., Reeves, J. M., Darbeheshti,  
904 M., Baumgardner, D. G., Kok, G. L., Chung, S. H., Schulz, M., Hendricks, J., Lauer, A., Kärcher, B., Slowik,  
905 J. G., Rosenlof, K. H., Thompson, T. L., Langford, A. Q., Loewenstein, M., and Aikin, K. C.: Single-particle  
906 measurements of midlatitude black carbon and light-scattering aerosols from the boundary layer to the lower  
907 stratosphere, *J. Geophys. Res.*, 111, D16207, doi:10.1029/2006JD007076, 2006.

908 Schwarz, J. P., Gao, R. S., Spackman, J. R., Watts, L. A., Thomson, D. S., Fahey, D. W., Ryerson, T. B., Peischl, J.,  
909 Holloway, J. S., Trainer, M., Frost, G. J., Baynard, T., Lack, D. A., de Gouw, J. A., Warneke, C., and Del Negro,  
910 L. A.: Measurement of the mixing state, mass, and optical size of individual black carbon particles in urban and  
911 biomass burning emissions, *Geophys. Res. Lett.*, 35, L13810, doi:10.1029/2008GL033968, 2008.

912 Shiraiwa, M., Kondo, Y., Iwamoto, T., and Kita, K.: Amplification of light absorption of black carbon by organic

913 coating, *Aerosol Sci. Technol.*, 44, 46–54, doi:10.1080/02786820903357686, 2010.

914 Slowik, J. G., Cross, E. S., Han, J. H., Kolucki, J., Davidovits, P., Williams, L. R., Onasch, T. B., Jayne, J. T., Kolb,  
915 C. E., and Worsnop, D. R.: Measurements of morphology changes of fractal soot particles using coating and  
916 denuding experiments: implications for optical absorption and atmospheric lifetime, *Aerosol Sci. Technol.*, 41,  
917 734–750, doi:10.1080/02786820701432632, 2007.

918 Sorensen, C. M.: The mobility of fractal aggregates: A review, *Aerosol Sci. Technol.*, 45, 765–779,  
919 doi:10.1080/02786826.2011.560909, 2011.

920 Taylor, J. W., Allan, J. D., Liu, D., Flynn, M., Weber, R., Zhang, X., Lefer, B. L., Grossberg, N., Flynn, J., and Coe,  
921 H.: Assessment of the sensitivity of core/shell parameters derived using the single particle soot photometer to  
922 density and refractive index, *Atmos. Meas. Tech.*, 8, 1701–1718, doi:10.5194/amt-8-1701-2015, 2015.

923 Wang, Q. Y., Huang, R. J., Cao, J. J., Han, Y. M., Wang, G. H., Li, G. H., Wang, Y. C., Dai, W. T., Zhang, R. J., and  
924 Zhou, Y. Q.: Mixing state of black carbon aerosol in a heavily polluted urban area of China: implications for  
925 light absorption enhancement, *Aerosol Sci. Technol.*, 48, 689–697, doi:10.1080/02786826.2014.917758, 2014.

926 Wang, Y. Y., Liu, F. S., He, C. L., Bi, L., Cheng, T. H., Wang, Z. L., Zhang, H., Zhang, X. Y., Shi, Z. B., and Li, W.  
927 J.: Fractal dimensions and mixing structures of soot particles during atmospheric processing, *Environ. Sci.*  
928 *Technol. Lett.*, 4, 487–493, doi:10.1021/acs.estlett.7b00418, 2017.

929 Wentzel, M., Gorzawski, H., Naumann, K. H., Saathoff, H., and Weinbruch, S.: Transmission electron microscopical  
930 and aerosol dynamical characterization of soot aerosols, *J. Aerosol Sci.*, 34, 1347–1370, doi:10.1016/S0021-  
931 8502(03)00360-4, 2003.

932 Wu, Y. F., Zhang, R. J., Tian, P., Tao, J., Hsu, S.-C., Yan, P., Wang, Q. Y., Cao, J. J., Zhang, X. L., and Xia, X. A.:  
933 Effect of ambient humidity on the light absorption amplification of black carbon in Beijing during January 2013,  
934 *Atmos. Environ.*, 124, 217–223, doi:10.1016/j.atmosenv.2015.04.041, 2016.

935 Wu, Y. F., Wang, X. J., Tao, J., Huang, R. J., Tian, P., Cao, J. J., Zhang, L. M., Ho, K.-F., Han, Z. W., and Zhang, R.  
936 J.: Size distribution and source of black carbon aerosol in urban Beijing during winter haze episodes, *Atmos.*  
937 *Chem. Phys.*, 17, 7965–7975, doi:10.5194/acp-17-7965-2017, 2017.

938 Zhang, R. J., Jing, J., Tao, J., Hsu, S.-C., Wang, G., Cao, J., Lee, C.-S.-L., Zhu, L., Chen, Z., Zhao, Y. and Shen, Z.:  
939 Chemical characterization and source apportionment of PM<sub>2.5</sub> in Beijing: Seasonal perspective. *Atmos. Chem.*  
940 *Phys.* 13, 7053–7074, doi:10.5194/acp-13-7053-2013, 2013.

941 Zhang, R. Y., Khalizov, A. F., Pagels, J., Zhang, D., Xue, H., Chen, J., and McMurry, P. H.: Variability in morphology,  
942 hygroscopic and optical properties of soot aerosols during internal mixing in the atmosphere, *Proc. Natl. Acad.*  
943 *Sci. USA*, 105, 10291–10296, doi:10.1073/pnas.0804860105, 2008.

944 Zhang, Y. X., Zhang, Q., Cheng, Y. F., Su, H., Kecorius, S., Wang, Z. B., Wu, Z. J., Hu, M., Zhu, T., Wiedensohler,  
945 A., and He, K. B.: Measuring the morphology and density of internally mixed black carbon with SP2 and  
946 VTDMA: new insight into the absorption enhancement of black carbon in the atmosphere, *Atmos. Meas. Tech.*,  
947 9, 1833–1843, doi:10.5194/amt-9-1833-2016, 2016.